Journal of Hydrology: Regional Studies 62 (2025) 102960

Contents lists available at ScienceDirect

Journal of Hydrology: Regional Studies

journal homepage: www.elsevier.com/locate/ejrh

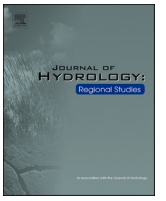

From global climate models to local water stress: A framework for estimating future water availability in the Mediterranean

Luis Garrote [a,*], Alvaro Sordo-Ward [a], Paola Bianucci [a], Francisco Martin-Carrasco [a], Ana Iglesias [b]

[a] Department of Civil Engineering, Hydraulics, Energy and Environment, Universidad Politécnica de Madrid, Madrid, Spain
[b] Department of Agricultural Economics, Statistics and Business Management, Universidad Politécnica de Madrid, Madrid, Spain

ARTICLE INFO

Keywords:
Water availability
Climate change
Mediterranean basin
Hydrological models
Water resources management
Climate scenarios

ABSTRACT

Study region: River basins draining into the Mediterranean Sea (excluding the Nile). The study area covers approximately 1.5 million km² across Southern Europe, North Africa, and the Near East, supporting around 200 million inhabitants.
Study focus: The objective is to assess potential water availability in Mediterranean basins under historical and future climate scenarios. Climate and runoff projections from the Inter-Sectoral Impact Model Intercomparison Project (ISIMIP3b) are combined with global hydrological models (H08 and CWatM) to simulate natural flows. The Water Availability and Adaptation Policy Analysis (WAAPA) model is used to incorporate reservoir operations, ecological flows, and demand reliability. Potential water availability is defined as the maximum demand that can be satisfied under specified management rules. The analysis considers three climate and socioeconomic scenarios (SSP1–2.6, SSP3–7.0 and SSP5–8.5) over two future time horizons (2020–2059 and 2060–2099).
New hydrological insights for the region: Results show a projected reduction of up to 26 % in annual flows and up to 41 % in potential availability by 2100 under high-emission scenarios. Reservoirs currently provide over 50 % of available water, buffering seasonal and interannual variability, yet increasing climate variability and population growth will exacerbate water stress. The study identifies spatial hotspots of future scarcity and emphasizes the need for basin-scale adaptation strategies and integrated management of surface, groundwater, and non-conventional water resources across the Mediterranean region.

1. Introduction

Water availability is a critical factor for socioeconomic development and ecosystem integrity, particularly in regions where climatic constraints intersect with high anthropogenic pressure. The Mediterranean basin is one such region, characterized by a marked seasonality of precipitation and peak water demand during the driest months. These features make it especially vulnerable to climate-induced changes in the water cycle, which threaten long-term water security (Iglesias et al., 2007; Sordo-Ward et al., 2019).

Water stress occurs when water demand persistently exceeds available supply, resulting in adverse impacts on human well-being

* Corresponding author.
E-mail addresses: l.garrote@upm.es (L. Garrote), alvaro.sordo.ward@upm.es (A. Sordo-Ward), paola.bianucci@upm.es (P. Bianucci), f.martin@upm.es (F. Martin-Carrasco), ana.iglesias@upm.es (A. Iglesias).

https://doi.org/10.1016/j.ejrh.2025.102960
Received 13 June 2025; Received in revised form 14 October 2025; Accepted 14 November 2025
Available online 18 November 2025

and aquatic ecosystems. Water stress in Mediterranean basins arises from both climatic and human factors. Limited water resources, strong seasonal variability, and intense agricultural and urban demands interact with the growing impacts of climate change, making these regions particularly vulnerable (Vörösmarty et al., 2010; Gain et al., 2016; Veldkamp et al., 2017). This study focuses specifically on the hydrological implications of climate change, which is essential to anticipate future imbalances between supply and demand, and to inform robust, adaptive management strategies.

An effective assessment of water stress requires dual consideration of hydroclimatic and socioeconomic variables. Traditional hydrological studies have largely focused on physical processes, such as rainfall, runoff, and streamflow, without adequately integrating demand-side dynamics. However, a more realistic depiction of water stress must incorporate variables such as population density, agricultural water use, consumption patterns, efficiency levels, and allocation priorities (Kummu et al., 2016; Liu et al., 2017). In Mediterranean regions, where irrigated agriculture and urban consumption increasingly compete for a finite resource, and where climatic extremes are expected to intensify, the need for such integrated approaches is particularly acute.

Water stress is often diagnosed through composite indices that synthesize pressure on water resources across large regions and timeframes. Among the most widely used is the Falkenmark indicator, based on per capita freshwater availability, due to its simplicity and scalability (Falkenmark et al., 1989). Complementary stress-based indices, such as the Water Stress Index (WSI) and the Water Exploitation Index (WEI), offer a more realistic approximation by explicitly comparing withdrawals to renewable supply (Pfister et al., 2009; Casadei et al., 2020). However, these indices often rely on annual averages that do not reflect the temporal variability of water availability and demand. In highly seasonal regions, short-term imbalances may cause severe shortages even when annual mean values suggest adequate supply (Raskin et al., 1997; Smakhtin et al., 2004).

Global hydrological models such as H08, CWatM, PCR-GLOBWB, and WaterGAP have been instrumental in identifying broad-scale water stress hotspots and in projecting the impacts of climate change on the continental and global scales (Wada et al., 2014; Zaherpour et al., 2018). However, they typically rely on standardized input datasets and simplified representations of water infrastructure and allocation rules, which may not accurately reflect the complex and highly regulated Mediterranean river systems. Conversely, regional models such as AQUATOOL (Andreu et al., 1996; Suárez-Almiñana et al., 2020), WEAP (Sieber and Purkey, 2015), or MODSIM (Labadie, 2006) can simulate operational and institutional complexity more precisely but are often less suited for long-term projections due to uncertainties about future infrastructure, operating rules, and socio-economic conditions. This context underscores the need for structurally simple yet conceptually robust models that can assess potential water availability under future climate scenarios, while minimizing dependence on parameters subject to change. Recent efforts have shown the value of such approaches, which combine stable physical features, such as river topology and reservoir location, with dynamic simulation of flow and demand (Paredes-Beltran et al., 2024; Bianucci et al., 2024).

Climate change is already altering the global water cycle, with profound implications for water availability, quality, and reliability. These impacts are especially visible in Mediterranean regions, where projections show increased aridity, more erratic precipitation, and increased drought risk (Seker et al., 2022; Vicente-Serrano et al., 2014; Cramer et al., 2018). These changes directly affect both surface and soil moisture (blue and green water), with critical consequences for agriculture and food security (Fader et al., 2016). Groundwater overexploitation, saline intrusion, and deteriorating water quality further exacerbate the vulnerability of the agricultural sector (Ben-Salem et al., 2023; Su et al., 2025; Dorado-Guerra et al., 2023).

The Sixth Assessment Report of the Intergovernmental Panel on Climate Change (IPCC, 2022) and the implementation of Shared Socioeconomic Pathways (SSPs) provide a coherent framework for assessing climate impacts under a range of future development and emissions trajectories (O'Neill et al., 2017). These scenarios are operationalized on model intercomparison platforms such as ISIMIP (Inter-Sectoral Impact Model Intercomparison Project), which delivers harmonized climate and hydrological datasets for global-scale impact assessments (Warszawski et al., 2014).

This study focuses on the river basins that drain into the Mediterranean Sea, excluding the Nile, covering an area of approximately 1.5 million km^2 and supporting a population of nearly 200 million people. These basins are characterized by a high level of human activity, urban, agricultural and industrial, and a dense network of reservoirs and infrastructure that mediate water allocation. Analyzing potential water availability in this region requires models that integrate climate projections, hydrological processes, and reservoir operation in a spatially explicit way.

Several recent review studies highlight the Mediterranean as a global hotspot for climate-induced water stress. Milano et al. (2013), Noto et al. (2023), and Iglesias and Garrote (2015) emphasize consistent trends of declining streamflow, groundwater recharge, and water security, particularly under high-emission scenarios. Similarly, Eekhout et al. (2025) and Arjdal et al. (2023) report robust declines in water availability using CMIP6 projections. Lionello and Scarascia (2018), Mariotti et al. (2015), and Tramblay et al. (2020) further confirm reductions in precipitation and increases in evapotranspiration, especially in southern Europe and North Africa. Collectively, these studies point to the urgent need for spatially detailed and operationally relevant analyses to inform climate adaptation in the Mediterranean.

Although these analyses provide valuable information on the expected evolution of the Mediterranean climate, their portrayal of water availability remains limited. In many cases, water availability is interpreted in purely climatological terms, typically equated with mean annual runoff over extended periods. However, in the context of water resource management, this definition is insufficient. Water is considered effectively available only if it can be supplied continuously and with a specified degree of reliability. Consequently, actual availability depends not only on long-term climatic averages, but also on the capacity of the hydrological system to regulate flows, manage temporal and spatial variability, and buffer against extreme events such as droughts. In addition, socioeconomic factors play a crucial role, particularly the ability to cope with water shortages, which is often governed by reliability thresholds that vary according to the type and priority of water use (e.g., urban supply, agriculture or environmental flows). Indices based on mean annual flow can thus mask the operational challenges of ensuring reliability and continuity of supply. This highlights a gap in the literature:

the need for operational indicators that integrate climate, infrastructure, and water allocation management to more accurately reflect regional vulnerabilities under climate change.

In this context, the present study proposes a simulation-based methodology to estimate potential water availability in Mediterranean basins, using climate and hydrological projections in combination with a water allocation model that accounts for reservoir regulation, evaporation losses, ecological flow requirements and demand priorities, providing a dynamic and spatially explicit estimate of available water. The main objective is to quantify how potential water availability evolves under historical conditions and future climate scenarios defined by the AR6 framework. Two global hydrological models (H08 and CWatM) are used to simulate natural flow inputs, which are then processed through a water resources management model to evaluate how reservoir infrastructure and management practices mediate supply availability across the basin network. By combining climate-hydrological modeling with realistic assumptions about water infrastructure and demand, this study aims to generate actionable information to support climate adaptation. The results offer a spatially explicit understanding of future water availability and identify priority areas for action. In addition, the proposed methodology can be extended to other basins facing similar challenges, contributing to larger efforts to enhance resilience in water-scarce regions under climate change.

The remainder of this paper is structured as follows. Section 2 presents the study area and describes the climate, hydrological, and socioeconomic data used in the analysis. It also presents the methodological framework, including the hydrological models (H08 and CWatM) and the WAAPA model used to simulate the potential availability of water under regulated conditions. Section 3 provides the main results of the study, including the validation of the global hydrological models, spatial and temporal patterns of projected runoff and water availability. Section 4 discusses key findings in light of the role of storage infrastructure, hydrological variability, and spatial disparities in water availability, highlighting implications for water management under climate change. Finally, Section 5 summarizes the main conclusions and proposes directions for future research and policy development.

2. Methodology

The methodology followed to assess the potential availability of water in the Mediterranean basins under future climate scenarios is organized in four phases: (1) collection and integration of spatial data, (2) collection of climate scenarios, (3) validation of global hydrological models and (4) estimation of potential water availability through simulation of water resources management.

2.1. Study area and data collection

The study area comprises the river basins that drain into the Mediterranean Sea, excluding the Nile River Basin. Geographically, these basins extend throughout Southern Europe, the Eastern Mediterranean, and North Africa, encompassing a diverse range of landscapes, from the mountainous catchments of the Alps and the Pyrenees to the semi-arid coastal plains of the Maghreb. Climatologically, the region is defined by the Mediterranean climate, characterized by warm, dry summers and mild, wet winters, although substantial gradients in temperature and precipitation exist due to topographic and latitudinal variability. Socioeconomically, the area

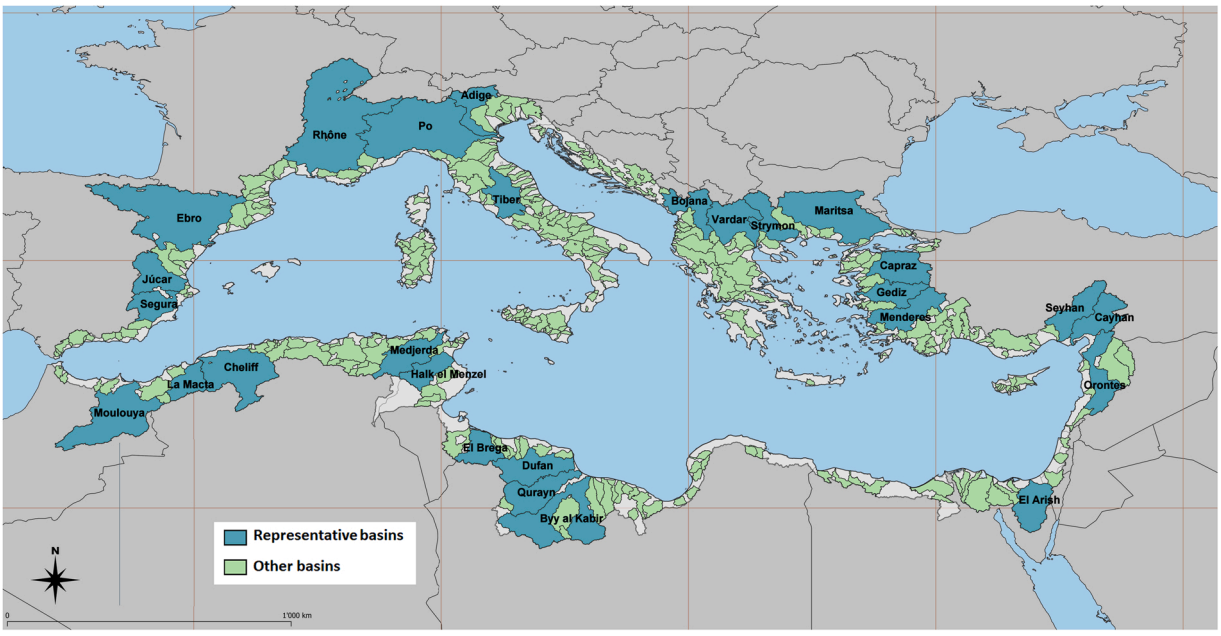

Fig. 1. Location of the study area and representative basins included in the analysis. Representative basins, for which detailed hydrological and performance indicators are reported, are highlighted and differentiated from the remaining basins.

includes both densely populated urban centers and agriculturally intensive rural zones, with high demand for water or irrigation, domestic consumption, and tourism. These pressures are compounded by growing vulnerability to climate change, particularly in semi-arid subregions. The Nile River Basin, while geographically connected to the southeastern edge of the Mediterranean, is excluded from the study due to its distinct hydrological and socio-economic context. Most Mediterranean basins are characterized by short river systems with headwaters in mountainous regions and strong seasonality linked to Mediterranean climatic regimes: The Nile, however, is a transcontinental river whose main sources lie far outside the Mediterranean climate zone, most notably in the tropical highlands of East Africa and the Ethiopian Plateau, and its catchment area is more than twice the size of all other Mediterranean basins combined. Its flow regime is dominated by monsoonal precipitation patterns and long-distance upstream contributions, resulting in hydrological dynamics that differ fundamentally from those of typical Mediterranean basins. Additionally, the socio-economic context of water use and governance in the Nile Basin, marked by complex international water-sharing disputes, differs markedly from the governance frameworks of most Mediterranean basins.

The study region is delineated in Fig. 1. For detailed analyses, we selected a set of Mediterranean-draining river basins with a contributing area of 14,000 km^2 or more, which are highlighted in teal color in the figure. These basins cover a total area of approximately 866,400 km^2, representing more than half of the entire Mediterranean coastal drainage area considered in this study, which is 1.5 million km^2.

To characterize the hydrological behavior and identify the analysis points, a GIS environment was implemented in which various data sources were integrated. The mapping support of the Mediterranean basins was configured using the 3-arcsecond hydrological products provided by HydroSheds, which is a database of topographic information of high resolution and global consistency (Lehner et al., 2008). Key hydrologic products include a digital elevation model, drainage directions, and flow accumulation rasters. The spatial support for the analysis of the Mediterranean basins is composed of all river sections with a catchment area of more than 1000 km^2 or located downstream of relevant reservoirs. A total of 3686 sub-basins were delimited, in 363 basins, with a total accumulated area of 1.495 million km^2. From the final drainage points of the basins, the river network was delineated, following the drainage direction, and structured into a network of nodes and sections. The following relevant points for analysis were identified: (1) headwaters, which are points with at most 1000 km^2 of catchment area that identify the beginning of the river network; (2) dams; (3) confluences of two rivers, where three nodes are identified: the last two nodes of the upstream sections and the first node of the downstream section; (4) intermediate nodes in sections that have an incremental basin above the threshold of 1000 km^2 and (5) final drainage points that flow into the sea.

Three primary data sources were used to compile information on dams and reservoirs: the World Register of Dams (WRD), the Global Reservoir and Dam Database (GRanD), and the GlObal geOreferenced Database of Dams (GOODD). The WRD, provided by the International Commission on Large Dams (ICOLD), is widely regarded as the most comprehensive global dam database, containing over 58,000 records (ICOLD, 2023). However, it does not include georeferenced locations for the dams. The GRanD dataset, compiled by Lehner et al. (2011), includes 6862 georeferenced records of reservoirs and their associated dams, with a cumulative storage capacity of 6197 km^3 . Reservoir outlines are provided as high-resolution polygons. Despite its spatial detail, the dataset is incomplete for the Mediterranean region. The GOODD dataset, developed by Mulligan et al. (2020), was created by manually digitizing visible dams using Google Earth satellite imagery. It contains over 38,000 dam locations globally, but provides only point locations, with no

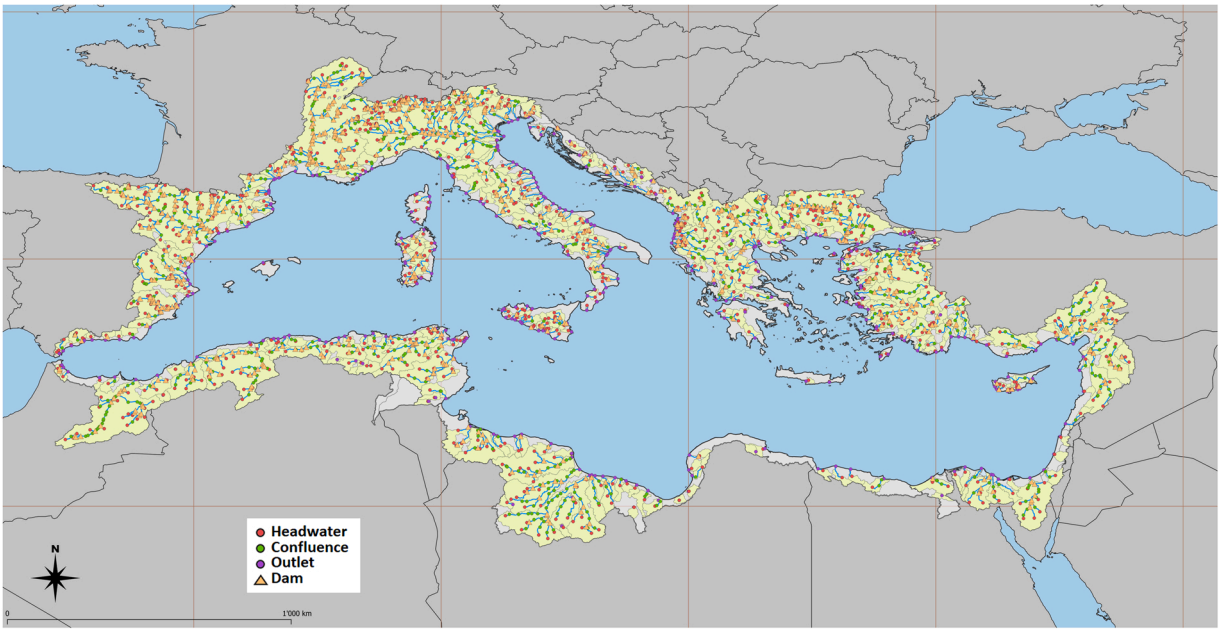

Fig. 2. Main components of the cartographic framework: River sections, basins and nodes (classified as headwater, confluence, outlet and dams).

associated reservoir or structural attributes.

To obtain comprehensive coverage for the study domain, the three datasets were merged and processed. Georeferencing was based on the GRanD and GOODD datasets, which respectively include 453 and 955 dams within the study area. These locations were cross-referenced with the WRD, which provides key attributes such as dam height and reservoir storage capacity. From the combined data set, dams with a storage capacity greater than 0.001 km^3 were selected and georeferenced using the HydroSHEDS flow accumulation layer. This resulted in a set of 839 dams, with a total storage capacity of 92.37 km^3 . For the purposes of modeling water availability, dams used exclusively for hydroelectric generation were excluded. This left 586 dams used primarily for regulation, with a useful storage volume of 67.64 km^3 .

The resulting network is a collection of 3731 nodes and 3668 river sections. There are 895 header nodes, of which 558 are occupied by dams. There are another 820 intermediate nodes, of which 281 are occupied by intermediate dams. There are 530 river confluences, which give rise to 1590 nodes (1060 upstream and 530 downstream). The network has 363 final drainage points along the Mediterranean coastline.

Fig. 2 shows the components of the constructed topological model. On the river network, the 3731 singular points of the calculation model have been represented by circles in the graph. The river sections between two consecutive nodes of the river network have been identified and the corresponding sub-basins have been delimited. The graph also shows the 839 reservoirs in the Mediterranean basins with a capacity of more than 0.001 km^3.

Socioeconomic variables were incorporated into the cartographic framework to help estimate pressure on water resources. Population data for each sub-basin were derived from the GRUMP (Global Rural-Urban Mapping Project), specifically using the Gridded Population of the World, Version 4 (GPWv4), Population Density for the year 2020 (CIESIN, 2017), at a spatial resolution of 2.5 arc-minutes (approximately 0.0417 °). According to this dataset, the total population within the Mediterranean basins amounts to 199.39 million inhabitants. Future population projections were sourced from the Global One-Eighth Degree Population Base Year and Projection Grids Based on the SSPs, v1.01 (Jones and O'Neill, 2017). This dataset provides global population grids at a resolution of 7.5 arc-minutes (0.125 °), aligned with the Shared Socioeconomic Pathways (SSPs) and designed for use in climate, socioeconomic, environmental, and related studies. It includes base year data for 2000 and decadal projections from 2010 to 2100. For this study, projection grids for the years 2020, 2040, and 2080 were selected under three SSP scenarios: SSP1 (sustainability), SSP3 (regional rivalry), and SSP5 (fossil-fueled development). The 2020 grid was used as a baseline to estimate population change for the 2040 horizon (representing the 2020–2059 period) and the 2080 horizon (representing the 2060–2099 period).

The irrigated area within each sub-basin was estimated using the Global Map of Irrigated Areas (GMIA), a set of irrigation-related mapping products developed by the FAO's Land and Water Division in collaboration with the Rheinische Friedrich-Wilhelms-Universität Bonn. The GMIA provides global raster datasets at a spatial resolution of 5 arc-minutes (~10 km), including several irrigation variables. For this study, the variable used was the area equipped for irrigation using surface water, representing areas where surface water is actually used for irrigation. The GMIA dataset is distributed by AQUASTAT, the FAO's global water information system (Siebert et al., 2013). According to this source, the total area effectively irrigated with surface water in the Mediterranean basins is approximately 5.92 million hectares. Together, the GRUMP dataset (for population distribution) and the GMIA dataset (for irrigated area) were used as indicators to characterize the spatial distribution of water demand drivers across the study area.

2.2. Compilation of climate scenarios

The climate scenarios used in this study were obtained from the ISIMIP3b project (Warszawski et al., 2014), which provides the climate inputs required to drive global hydrological models and generate streamflow simulations under various AR6 emission scenarios: SSP1–2.6, SSP3–7.0, and SSP5–8.5. The climate scenarios analyzed in this paper are summarized in Table 1. Two main categories of climate scenarios were considered: past and future. The past category includes two types of simulations: (1) *obsclim*, in which hydrological models are forced with observed climate data, typically derived from reanalysis products; and (2) *historical*, in which hydrological models are driven by climate model simulations for the historical period, enabling consistent comparisons with future projections. The future scenarios: *ssp126*, *ssp370*, and *ssp585*, correspond to the AR6 Shared Socioeconomic Pathways: SSP1–2.6 (sustainability), SSP3–7.0 (regional rivalry), and SSP5–8.5 (fossil-fueled development). In these simulations, climate models are forced

Table 1
Climate scenarios collected from the ISIMIP3b project.

Climate scenario	Climate models	Period
obsclim: models forced with the observed weather in the real sequence	GSWP3	1900–2019
historical: models forced with simulated weather under historical conditions	GFDL-ESM	1850–2014
	MRI-ESM	
	IPSL-ESM	
	MPI-ESM	
	UKSM-ESM	
ssp126: models forced with the simulated climate in the SSP1–2.6 emissions scenario	GFDL-ESM	2015–2100
ssp370: models forced with the simulated climate in the SSP3–7.0 emissions scenario	MRI-ESM	
ssp585: models forced with the simulated climate in the SSP5–8.5 emissions scenario	IPSL-ESM	
	MPI-ESM	
	UKSM-ESM	

with greenhouse gas emissions specific to each scenario, and the resulting climate outputs are used to drive the hydrological models.

The *obsclim* scenario refers to an observational climate dataset used primarily for comparison and validation purposes. It represents a set of observed climate conditions, typically derived from historical climate records, reanalysis products, and other observational sources. In ISIMIP3b, the *obsclim* scenario is based on the GSWP3 (Global Soil Wetness Project Phase 3) dataset (Weedon et al., 2014) and serves as a reference or baseline against which the performance of climate model simulations and impact assessments can be evaluated. The simulation period available for *obsclim* in ISIMIP3b spans 1900–2019. The *historical* scenario, by contrast, represents the past climate as simulated by global climate models under historical greenhouse gas concentrations and forcings. Unlike *obsclim*, the historical scenario does not reproduce the exact sequence of observed weather events but reflects the internal variability and response of each model to historical greenhouse gas emission forcing. This scenario is useful for assessing the consistency and evolution of model simulations over the past century.

The results from five global climate models (GCMs) were used in this study. These models, developed by leading climate research institutions, represent state-of-the-art tools for simulating the Earth's climate system:

1. GFDL-ESM: Developed by the Geophysical Fluid Dynamics Laboratory (GFDL) of the U.S. National Oceanic and Atmospheric Administration (NOAA), this model integrates atmospheric, oceanic, terrestrial, and biogeochemical processes to simulate Earth system dynamics (Dunne et al., 2020).
2. MRI-ESM: Created by the Meteorological Research Institute (MRI) of Japan, this Earth system model is designed to investigate climate variability and change by representing key components of the climate system, including atmosphere, ocean, and land processes (Yukimoto et al., 2011).
3. IPSL-ESM: Developed by the Institut Pierre-Simon Laplace (IPSL) in France, this model incorporates the atmosphere, ocean, land surface, and sea ice, along with biogeochemical cycles, to simulate long-term climate evolution (Sepulchre et al., 2020).
4. MPI-ESM: Developed by the Max Planck Institute for Meteorology in Germany, this model emphasizes interactions among the atmosphere, ocean, land, and sea ice, enabling detailed simulations of climate feedbacks at both regional and global scales (Gutjahr et al., 2019).
5. UKESM: Produced by the UK Met Office Hadley Centre, in collaboration with other UK research institutions, the UK Earth System Model (UKESM) extends a traditional atmosphere-ocean general circulation model with terrestrial and oceanic biogeochemistry and carbon cycle components (Sellar et al., 2019).

The *historical* scenario is used as a reference in climate model simulations and impact assessments to represent climate conditions over a defined period in the recent past. In ISIMIP3b, this scenario covers the period 1850–2014.

The SSP1–2.6 (*ssp126*), SSP3–7.0 (*ssp370*), and SSP5–8.5 (*ssp585*) scenarios correspond to specific Shared Socioeconomic Pathways (SSPs) used in climate modeling and impact assessments. These scenarios represent distinct trajectories of future greenhouse gas emissions and socioeconomic development, reflecting a range of possible climate futures. The same five global climate models used for the *historical* simulations were employed to generate projections under these future scenarios. Within the ISIMIP3b framework, the available simulation period for future scenarios spans 2015–2100.

The *obsclim* scenario is particularly valuable for validating hydrological model outputs against observational data and for characterizing the historical evolution of water availability. Comparing the *obsclim* and historical scenarios allows for an assessment of how well climate models reproduce the observed climate response to past greenhouse gas emissions. In turn, the impacts of future climate change can be evaluated by comparing projections under the *ssp126*, *ssp370*, and *ssp585* scenarios with the *historical* baseline.

For the purposes of this study, projections were analyzed across four time windows: (1) Observation period: 1980–2019; (2) Historical reference period: 1975–2014; (3) Near-future period: 2020–2059; and (4) Distant-future period: 2060–2099.

Given that the Mediterranean region spans parts of three continents, the study area encompasses a vast and geographically diverse domain. In the absence of high-resolution regional hydrological models that consistently cover this entire transcontinental area, global hydrological models were selected to simulate natural streamflow under historical and future climate conditions. These models provide comprehensive, consistent, and spatially continuous hydrological simulations on the global scale, making them appropriate tools for assessing water availability across the entire Mediterranean basin. Two global hydrological models from the ISIMIP3b project were selected for this study: H08 and CWatM. H08 is a process-based global hydrological model that simulates the terrestrial water cycle by accounting for key physical processes such as precipitation, evapotranspiration, infiltration, runoff generation, and river routing. It comprises six submodules: surface hydrology, river routing, reservoir operations, crop growth, environmental flow requirements, and water withdrawal. Detailed model formulations are provided in (Hanasaki et al., 2008; Hanasaki et al., 2010). CWatM (Community Water Model) is a spatially distributed global hydrological model designed to assess the impacts of climate change on water resources, including runoff, river discharge, and soil moisture. It simulates rainfall-runoff processes and water routing through river networks (Burek et al., 2020).

Both H08 and CWatM were calibrated and validated by their respective development teams using globally consistent datasets. For H08, calibration and parameter inference were carried out by Yoshida et al. (2022), who optimized climate-based parameters using a Bayesian Markov Chain Monte Carlo (MCMC) approach across more than 400 large river basins worldwide. The model was calibrated against monthly discharge data from the Global Runoff Data Centre (GRDC). The evaluation of results showed Nash-Sutcliffe Efficiency (NSE) values typically between 0.60 and 0.85, percent bias (PBIAS) within ±15 %, and Kling-Gupta Efficiency (KGE) values between 0.65 and 0.80, indicating good overall skill in reproducing historical river discharge at large scales. The CWatM model was calibrated using a comparable approach based on discharge observations from more than 3000 GRDC stations, as described by Burek et al. (2020) and Burek and Smilovic (2023). Calibration was conducted through regional parameter transfer and multi-basin optimization,

ensuring consistent model behavior across diverse hydroclimatic regions. Reported validation statistics include median NSE values between 0.65 and 0.80, median KGE around 0.70, and PBIAS typically below ±20 %.

These models were used to simulate natural water flow at the nodes of the Mediterranean basin model under both historical and future climate conditions. Both H08 and CWatM are driven by climate input data from the ISIMIP3b framework and produce runoff at a spatial resolution of 0.5° × 0.5°, incorporating sub-grid variability to account for topography and land cover, and use a daily time step. The spatial resolution of the global hydrological models corresponds to grid cells of approximately 800–1000 km² in the Mediterranean region. Although this represents a relatively coarse spatial resolution, the sub-basins of the spatial support are of comparable size, with an average area of 400 km². Runoff values were interpolated from the global model grids to the 3-arcsecond high-resolution grid using a distance-weighted algorithm previously validated by González-Zeas et al. (2012) for improving runoff estimates from regional climate models. These runoff values were then aggregated to compute monthly streamflow series at key nodes along the river network, corresponding to each of the climate scenarios analyzed in the study.

Table 2 presents a summary of key physical and socioeconomic characteristics for each of the major river basins included in the study. For each basin, the following variables are reported: total contributing area, mean annual flow, number of dams, total reservoir storage capacity, population and irrigated area.

2.3. Validation of global hydrological models

Before applying the global H08 and CWatM models to assess water availability in the Mediterranean region, their outputs were evaluated against results from high-resolution national hydrological models that provide more locally calibrated simulations. Specifically, the SIMPA model was used for river basins in Spain and the BIGBANG model for those in Italy. The SIMPA model (Integrated System for Precipitation-Runoff Modeling) simulates the hydrological behavior in the natural regime in Spanish river basins (Estrela and Quintas, 1996). It is a conceptual and distributed model that operates on a monthly scale on a regular grid of 500 × 500 m and covers the entire Spanish territory. Its conceptual structure combines a water balance model with a runoff scheme based on regionally calibrated parameters. The most recent version of the model and its application to Spanish basins is described in (CEDEX, 2020). BIGBANG, developed by the Italian Institute for Environmental Protection and Research (ISPRA), is a high-resolution distributed model used for national-scale hydrological assessments in Italy. Designed to evaluate the components of the hydrological water budget across Italy, BIGBANG operates on a regular grid with a spatial resolution of 1 km and provides monthly estimates of key variables such as precipitation, actual evapotranspiration, surface runoff, and groundwater recharge (Braca et al., 2022). The model integrates high-resolution climatic, soil, and land-use data within a GIS framework, enabling detailed assessments of water resource availability and drought conditions at national and regional scales. The application of BIGBANG to Italian basins is described in (Braca et al., 2021).

These models were calibrated using detailed local data and knowledge and provide more reliable estimates of natural flow

Table 2
Relevant variables of the main basins in the study area.

Basin	Area	Flow	Dams	Storage	Population	Irrigated
	1000 x km²	km³/yr	number	km³	M hab	1000 x ha
Rhone	95.75	54.30	35	4.01	12.06	179.99
Ebro	84.63	14.60	54	6.66	3.76	602.27
Po	73.33	41.83	10	0.96	18.89	928.83
Moulouya	54.19	2.53	2	0.44	1.31	53.98
Maritsa	52.48	8.42	39	3.42	3.42	115.14
Bayy al Kabir	52.36	0.43	0	0.00	0.14	0.00
Cheliff	44.31	2.57	13	1.92	5.49	41.30
Dufan	29.37	1.04	0	0.00	0.54	0.05
Qurayn	28.92	0.36	0	0.00	0.30	0.00
Vardar	24.49	3.50	10	1.17	1.66	89.26
Menderes	24.33	5.09	12	2.56	2.28	153.03
Capraz	23.73	5.01	12	1.27	3.68	61.49
El Arish	23.72	0.13	0	0.00	0.16	0.04
Orontes	23.68	5.23	3	0.46	6.50	136.92
Medjerda	23.13	3.43	11	1.36	2.37	64.35
Jucar	21.38	1.81	5	2.47	0.95	61.90
Cayhan	21.20	5.14	8	3.52	2.14	148.49
Seyhan	20.72	3.58	3	1.57	1.39	63.92
Bojana	17.18	11.04	2	0.12	1.75	49.94
Strymon	16.78	2.03	8	0.23	0.87	82.22
Gediz	16.76	3.08	5	1.61	1.88	66.86
Tiber	16.69	5.88	3	0.36	4.75	29.77
Segura	16.57	0.92	18	1.14	1.78	102.76
El Brega	16.43	1.02	0	0.00	0.38	0.03
Halk el Menzel	15.25	0.69	4	0.41	1.23	23.18
La Macta	14.58	0.50	4	0.21	2.13	24.28
Adige	14.42	7.01	0	0.00	2.05	102.00

conditions than direct observations, which are often influenced by human alterations. As such, they are well-suited for evaluating the performance of global hydrological models in the Mediterranean context. This validation step was essential to account for the differences in spatial resolution between models and to ensure that global simulations adequately capture hydrological behavior at the basin scale. The comparison included analyses of both annual and monthly flow series, supported by statistical performance indicators. The following indicators were used:

The percentage of bias (*PBIAS*) is a commonly used statistical indicator to evaluate the performance of hydrological models by measuring the average tendency of simulated values to be larger or smaller than observed (or reference) values. It is calculated as follows:

$$PBIAS = 100 * \frac{\sum_{i=1}^{n} (S_i - O_i)}{\sum_{i=1}^{n} O_i}$$

Where:

S_i: annual flow value simulated by the global models for year i

O_i: annual flow values simulated using the SIMPA or BIGBANG model year i

n: number of years in the series.

The Nash-Sutcliffe coefficient of efficiency (*NSE*) is a widely used statistical metric to assess the predictive skill of hydrological models by quantifying how well the simulated data matches the observed (or reference) data over time (Nash and Sutcliffe, 1970). It is calculated as follows:

$$NSE = 1 - \frac{\sum_{i=1}^{n} (O_i - S_i)^2}{\sum_{i=1}^{n} (O_i - \mu_o)^2}$$

Where:

μ_o: average value of the annual flows of the SIMPA or BIGBANG model.

The perfect fit corresponds to $NSE = 1$. If $NSE < 0$, the behavior of the model is worse than the use of the average of the observed data. *NSE* is commonly used to evaluate how well a hydrological model reproduces the temporal dynamics of streamflow or other hydrological variables. It emphasizes the model's ability to capture both the magnitude and timing of flows, making it a robust indicator of model performance over the entire simulation period.

The Kling-Gupta efficiency coefficient (*KGE*) is a performance metric designed to provide a balanced evaluation of hydrological model accuracy by combining correlation, bias, and variability into a single measure. It was proposed by Kling and Gupta in 2009 (Gupta et al. 2009), to improve some limitations of the Nash-Sutcliffe coefficient (*NSE*). It is calculated as follows:

$$KGE = 1 - \sqrt{(r-1)^2 + \left(\frac{\mu_s}{\mu_o} - 1\right)^2 + \left(\frac{\sigma_s}{\sigma_o} - 1\right)^2}$$

Where:

r: Pearson correlation coefficient between the annual flows of the global hydrological models and those of the SIMPA or BIGBANG model.

μ_s: average value of the annual flows of the global models.

σ_s: standard deviation of the annual flows of the global models.

σ_o: standard deviation of the annual flows of the SIMPA or BIGBANG model.

The perfect fit corresponds to $KGE = 1$. Values closer to 1 indicate better agreement between simulated and observed data in terms of timing, magnitude, and variability. Lower values indicate poorer model performance. *KGE* is widely used for hydrological model evaluation because it provides a comprehensive assessment of model performance, overcoming some limitations of other metrics like *NSE* by explicitly separating correlation, bias, and variability components. This makes it a valuable tool for understanding different aspects of model behavior when simulating streamflow or other hydrological variables.

2.4. Assessment of potential water availability

The model used in this study to assess potential water availability is called WAAPA (Water Availability and Adaptation Policy Analysis). WAAPA provides a general framework for analyzing reservoir regulation within water resources systems. Its core components include reservoirs, inflows, and water demands, all of which are linked to specific nodes within the river network. The model simulates reservoir operations and calculates water supply to demands from individual reservoirs or integrated reservoir systems, while accounting for ecological flow requirements and evaporation losses. By analyzing the time series of volumes delivered to demands, WAAPA enables the calculation of supply reliability using various performance criteria. The model is flexible and can be applied in different ways: it can simulate the operation of a system under known demand conditions, or it can estimate key operational metrics through iterative algorithms that repeat the basic simulation procedure. For example, WAAPA can generate a demand-

reliability curve, which illustrates the relationship between the magnitude of water demand and the reliability with which it can be met. This curve is fundamental for determining the potential water availability based on a specified reliability criterion. It should be noted that this water availability refers exclusively to surface water resources as represented by the WAAPA model. Groundwater dynamics are not explicitly simulated. The assessment of water availability therefore captures the potential supply from river flows and reservoir storage but does not include contributions from aquifers or non-conventional sources such as desalinated or reclaimed water.

The input data for WAAPA include the river network topology, which specifies the locations of reservoirs, the inflows at key points within the network, basin water demands, ecological flow requirements, and detailed reservoir characteristics. Demands are categorized by type and prioritized accordingly. For each demand, the model requires information on its annual variation (modulation) and the return flow coefficient, representing the portion of water returned to the system after use. Reservoir data include the maximum and minimum storage capacity for each month, the relationship between storage volume and flooded surface area and monthly evaporation rates.

The model simulates the water flow at each node of the river network. When a node contains a reservoir, its operation is modeled using a conventional regulation algorithm that proceeds through several steps during each time period. First, the algorithm attempts to satisfy the ecological flow requirement with the incoming water. If the inflow is insufficient, a deficit occurs because no water can be released to meet this ecological demand. Then, evaporation losses are calculated based on the flooded surface area of the reservoir, and the available storage volume is adjusted accordingly. Then, the remaining inflow, after accounting for ecological flow, is added to the storage of the reservoir. The water demands are supplied in priority order whenever possible, and the storage volume is updated after these demands are met. If the storage volume exceeds the maximum capacity of the reservoir, the excess water is released through the spillway. These reservoir operation rules are simplified to maximize local water availability, as detailed and harmonized data on coordinated reservoir management, inter-reservoir operation, and drought contingency protocols are not publicly available for the entire region. The actual behavior of the reservoir often deviates from this idealized operation, especially under drought conditions, when ecological releases may be suspended or reduced once storage falls below warning thresholds. For nodes without reservoirs, the same algorithm is applied, but with zero storage capacity and no evaporation losses considered.

In this study, potential water availability is defined as the maximum demand that can be met at a given point in the river network, accounting for existing regulation infrastructure and adhering to management constraints such as ecological flow requirements, reservoir operating rules, evaporation losses, monthly demand variations, and the specified reliability criterion. It is important to emphasize that, under this definition, potential water availability is not a fixed value; rather, it varies depending on the allocation to ecological flows, the type of demand considered, the operational rules in place, and the reliability criterion applied.

The potential availability of water, understood as the maximum allowable demand, is calculated for each node in the basin's data structure. The inputs required include the monthly distribution of demand, the presence of return flows, the reliability criterion to be applied, failure threshold values, and acceptable levels of supply reliability. At each node, the WAAPA model uses an iterative algorithm that begins with an initial demand set equal to the average annual flow at that location. The system is then simulated to evaluate whether the resulting supply reliability meets the predefined criterion. If the criterion is not met, the demand is reduced; if it is exceeded, the demand is increased. With each iteration, the adjustment to the demand is halved to improve convergence. The process continues until the change in demand falls below a defined precision threshold. The final demand value that satisfies the reliability criterion is identified as the maximum allowable demand for that river segment under the given management conditions.

In the simulation of the entire flow network, the maximum allowable demand for all nodes of a given basin is determined by sequentially applying the procedure described above. Under the management assumption adopted in this study, local management, the algorithm is applied node by node to calculate the maximum demand that can be supplied using the operation model of the individual reservoir associated with each node. For each node, it is assumed that the maximum allowable demand has already been computed for all upstream nodes. The local algorithm then determines the maximum demand that can be reliably supplied at the current node, considering the presence of a local reservoir, if applicable. The inflow to the reservoir is computed as the sum of the ecological flows and controlled spills from immediately upstream reservoirs, plus the contribution from the local sub-basin. The algorithm proceeds recursively throughout the network, always processing the upstream nodes before their downstream counterparts. As the simulation progresses downstream, local demands are accumulated, allowing the model to compute the maximum allowable demand at each node within the entire river network. This maximum allowable demand is identified as the potential water availability in this study.

The WAAPA model allocates water resources within the boundaries of each hydrological basin, assuming that the supply and demand nodes are internally connected through the natural drainage network. Due to the absence of spatially explicit and harmonized data on interbasin transfer systems and operational conveyance rules for the entire Mediterranean region, the model does not explicitly simulate artificial water transfers across basin boundaries. This simplification implies that all water use (urban, agricultural, and environmental) is supplied from sources located within the same hydrological unit. Although this approach may introduce local inaccuracies in areas with large transfer infrastructures (e.g., major cities or irrigated districts supplied from external basins), its effect diminishes at larger scales, where the aggregation of sub-basins captures the integrated water balance of the drainage system (Eng et al., 2025).

Water availability is strongly influenced by the temporal distribution of demand throughout the year. Urban supply typically exhibits limited seasonal variation, except in regions with marked seasonal activity, such as those influenced by tourism. In contrast, irrigation demand exhibits pronounced intra-annual variability. It peaks in the dry months, opposing the natural hydrological regime and thereby imposing strong constraints on water availability. In this study, the model was configured to simulate a composite demand composed of 20 % urban and 80 % agricultural use, reflecting average conditions across Mediterranean basins (Harmanny and Malek, 2019; Plan Bleu, 2008). Return flows were not considered; all water allocated to demands is treated as withdrawn from the system. The supply reliability criterion applied follows Spanish irrigation regulations, which define a mixed reliability standard based on

cumulative annual deficits over different time horizons. Demand is considered satisfactorily met when the following three conditions are simultaneously fulfilled: (1) the maximum annual deficit does not exceed 50 % of the annual demand; (2) the maximum two-year cumulative deficit does not exceed 75 % of annual demand; and (3) the maximum cumulative deficit over any ten-year period does not exceed 50 % of annual demand.

The WAAPA model simulates water allocation at a monthly time step, assigning available water to different uses following general priority rules. Although the model includes functionality to specify environmental flow requirements for each river reach, this feature was not applied in the present analysis due to the absence of harmonized data on ecological flow criteria, magnitudes, and priority hierarchies across Mediterranean countries. Therefore, the results presented correspond to gross potential water availability, which should be interpreted as the upper limit of the resource before environmental allocations are considered.

The WAAPA model was applied at the nodes defined in the cartographic framework, generating estimates of water availability at each point in the river network. The results are presented by displaying, at each node, the cumulative water availability across all upstream nodes within the corresponding catchment area. This approach allows to produce high-resolution maps that illustrate spatial patterns of potential water availability for each of the analyzed time periods.

The concept of potential water availability, as computed in this study, refers to the maximum volume of water that can be sustainably supplied at each node along the river network under the defined management assumptions. While this availability is calculated at specific locations within the fluvial system, its interpretation should not be limited to the immediate surroundings of the river. Water can be conveyed from these nodes to supply demands located nearby or even at considerable distances, provided that the necessary infrastructure is available and operational. Therefore, potential water availability should not be interpreted as the actual amount of water allocated to meet current or future demands, but rather as a theoretical upper limit of the system's capacity to provide water with an acceptable level of reliability. In areas where existing demands are below this potential availability, water requirements could be met without significant deficits, leaving part of the resource to be used downstream. Conversely, where actual demands exceed potential availability, shortages beyond the admissible reliability thresholds can be expected. Therefore, potential water availability should be regarded as a reference indicator for assessing the sustainability of water management and identifying zones where the resource may become critically limiting under future conditions.

Potential water availability represents the geographical distribution of available water that can support a broader assessment of regional supply-demand balances. When integrated with information on infrastructure capacity and spatial distribution of demands, it becomes a valuable tool for evaluating the feasibility of meeting existing or projected water needs in a territory.

It is also important to note that the total potential availability estimated for each basin must be subsequently allocated among the different water uses: environmental, urban, agricultural, and others. For this reason, the indicators expressed per inhabitant and per irrigated hectare provide complementary perspectives and should not be summed directly, as they reflect distinct but overlapping components of the same total resource.

3. Results

The presentation of results is organized into four main sections to ensure a coherent and comprehensive analysis: (1) evaluation of the consistency between the outputs of global hydrological models and high-resolution local data on natural flow; (2) presentation of simulated streamflow and potential water availability across all Mediterranean basins under different climate scenarios; (3) analysis of the temporal evolution of these indicators throughout the twenty-first century; and (4) assessment of the spatial distribution of streamflow and water availability across the Mediterranean basin.

3.1. Assessing consistency between global hydrologic models and local hydrologic information

Before applying the global hydrological models to future projections, a comparative evaluation of their performance in simulating natural streamflow during the historical period was conducted. As a reference, we used the monthly flow series generated by the high-resolution SIMPA model in Spain and the BIGBANG model in Italy. This validation step was essential, given the greater spatial detail and regional calibration of SIMPA and BIGBANG, which offer more accurate representations of local hydrological conditions than the coarser-resolution global models H08 and CWatM.

The presentation of the validation results was structured in three complementary stages to provide a comprehensive assessment of the performance of the global hydrological models. First, a detailed analysis was carried out for the two largest Mediterranean basins with high-quality reference data: the Ebro in Spain and the Po in Italy. This included visual inspection of annual and monthly flow series and performance metrics. Second, model performance was evaluated using statistical indicators, such as the percentage of bias (*PBIAS*), Nash-Sutcliffe efficiency coefficient (*NSE*), and Kling-Gupta efficiency coefficient (*KGE*), in a set of representative basins across Spain and Italy, where high-resolution validation data from SIMPA and BIGBANG were available. Finally, an aggregated comparison was performed based on average annual flows across all available basins in the region to identify broader patterns of model behavior and consistency.

The upper panel of Figure S1 illustrates the temporal evolution of annual streamflow simulated by the H08 and CWatM global hydrological models, compared to the reference series produced by the SIMPA model for the Ebro River, over the period 1940–2019, and the BIGBANG model for the Po River, over the period 1951–2022. Despite differences in model architecture, spatial resolution, and calibration, the global models capture the interannual variability of flows in both basins with reasonable fidelity. Nonetheless, some discrepancies are apparent in specific years, which can be attributed to the coarser resolution of the global models and differences in their internal process representations.

The lower panel of Figure S1 displays scatter plots comparing the annual flows generated by each global model with those produced by the SIMPA and BIGBANG models for the Ebro and Po Rivers, respectively. For the H08 model, the fit is excellent in the Po River, with a regression slope of 1.04, indicating a near-perfect agreement. In the Ebro River, H08 slightly underestimates flows, with a slope of 0.87. In both cases, the coefficient of determination is high ($R^2 = 0.987$), showing a strong temporal correlation between the simulated and reference series. However, it should be noted that a high R^2 alone does not imply full model agreement, as it mainly reflects the correspondence in the interannual variability of wet and dry years rather than the absence of bias. In contrast, the CWatM model shows better agreement with the Ebro River, yielding a regression slope close to unity (1.02), while slightly overestimating flows in the Po River, with a slope of 1.13. The R^2 values are also very high (0.994 for the Ebro and 0.986 for the Po), indicating that both models reproduce the temporal pattern of flows consistently with the local models. Taken together with the other performance metrics (*PBIAS*, *NSE*, *KGE*), these results confirm a good overall performance of the global hydrological models in these two large basins, especially considering their much coarser spatial resolution compared to the regional models used for validation. Overall, the performance of the global hydrological models in these two large basins is very good, especially considering their much coarser spatial resolution compared to the regional models used for validation.

At the monthly scale, the comparison of seasonal averages and the statistical distribution of monthly flows (Figure S2) shows that both global models successfully capture the characteristic seasonality of each basin, although some discrepancies remain in the reproduction of extreme values. Overall, CWatM aligns well with the seasonal pattern and variability observed in the SIMPA model for the Ebro River, accurately reflecting both the shape and dispersion of the monthly flow distribution. In contrast, H08 demonstrates a better fit to the distribution generated by the BIGBANG model for the Po River, particularly in reproducing the seasonal flow dynamics typical of this basin.

Table 3 presents the values of the performance indicators used to evaluate the ability of the global hydrological models H08 and CWatM to simulate annual flows in the main Mediterranean basins with a contributing area greater than 14,000 km^2. The table includes the Ebro, Júcar, and Segura basins in Spain, and the Po, Tiber, and Adige basins in Italy. For each case, the table reports the values of the percentage of bias (*PBIAS*), the Nash-Sutcliffe efficiency coefficient (*NSE*), and the Kling-Gupta efficiency coefficient (*KGE*), and the slope and coefficient of determination (R^2) of the regression line between simulated and reference annual flows. The results show that performance tends to be better in larger and wetter basins, such as the Italian basins and the Ebro, where indicators reach high levels of agreement with the reference data. In contrast, semiarid basins like the Júcar and especially the Segura exhibit noticeably lower performance, particularly for the H08 model, which produces a markedly low *NSE* value in the Segura basin. These differences highlight the challenges global models face in capturing the hydrological dynamics of smaller, highly regulated, or water-scarce basins, where local conditions exert a greater influence and are less well represented at coarse spatial resolution.

Fig. 3 presents two scatterplots that summarize the performance of the global hydrological models across all available basins in Spain (29) and Italy (92). The upper panel shows the relationship between the mean annual flows simulated by the global models and those obtained from the local reference models (SIMPA and BIGBANG), while the lower panel plots the percentage bias (*PBIAS*) against basin area. Results for the H08 model are presented on the left and results for the CWatM model are presented on the right. To accommodate the wide variation in basin sizes, plots are shown on a logarithmic scale. To aid interpretation, reference lines indicating

±25 % deviation from perfect agreement have been included in both plots.

The results illustrated in Fig. 3 reveal a clear trend: model performance tends to degrade in smaller basins, with a noticeable bias towards underestimation of flows. This pattern is expected given the coarse spatial resolution of global hydrological models, which limits their ability to capture the hydrological dynamics of smaller catchments. For the H08 model, 40 basins fall within the ±25 % error range, while in 80 basins the model underestimates flow by more than 25 %, and in only one case does it overestimate by more than 25 %. The CWatM model shows somewhat better overall performance: 50 basins lie within the ±25 % range, 57 basins exhibit underestimation beyond 25 %, and 14 basins show overestimation above this threshold. These findings underscore the limitations of global models in representing local hydrological behavior, particularly in smaller basins. Nevertheless, these models are designed to simulate the entire globe, and the lack of alternative streamflow data sources at the regional scale makes them a necessary reference. While results for smaller basins should be interpreted with caution, the strong agreement observed in larger basins is encouraging and suggests that global models are suitable for the estimation of natural flows in the Mediterranean basins within the framework of

Table 3
Performance indicators for the global hydrologic models in the relevant basins.

Basin	Model	PBIAS (%)	NSE	KGE	Slope	R^2
Ebro	H08	−13.2211	0.5391	0.7866	0.8707	0.9866
	CWatM	1.2699	0.6646	0.8105	1.0202	0.9939
Po	H08	4.5226	0.8427	0.8257	1.0362	0.9866
	CWatM	14.9936	0.8134	0.8236	1.1275	0.9861
Júcar	H08	19.4694	0.4564	0.4543	1.2154	0.9640
	CWatM	52.8399	0.6327	0.0372	1.5443	0.9691
Tiber	H08	−29.7400	0.6498	0.5239	0.6858	0.9629
	CWatM	−17.6268	0.5787	0.5661	0.7875	0.9622
Segura	H08	−0.4888	−0.0884	0.6694	1.0123	0.9590
	CWatM	30.5670	0.5415	−0.0284	1.3510	0.9279
Adige	H08	12.0933	0.9340	0.7620	1.0966	0.9850
	CWatM	16.5013	0.9285	0.7657	1.1347	0.9829

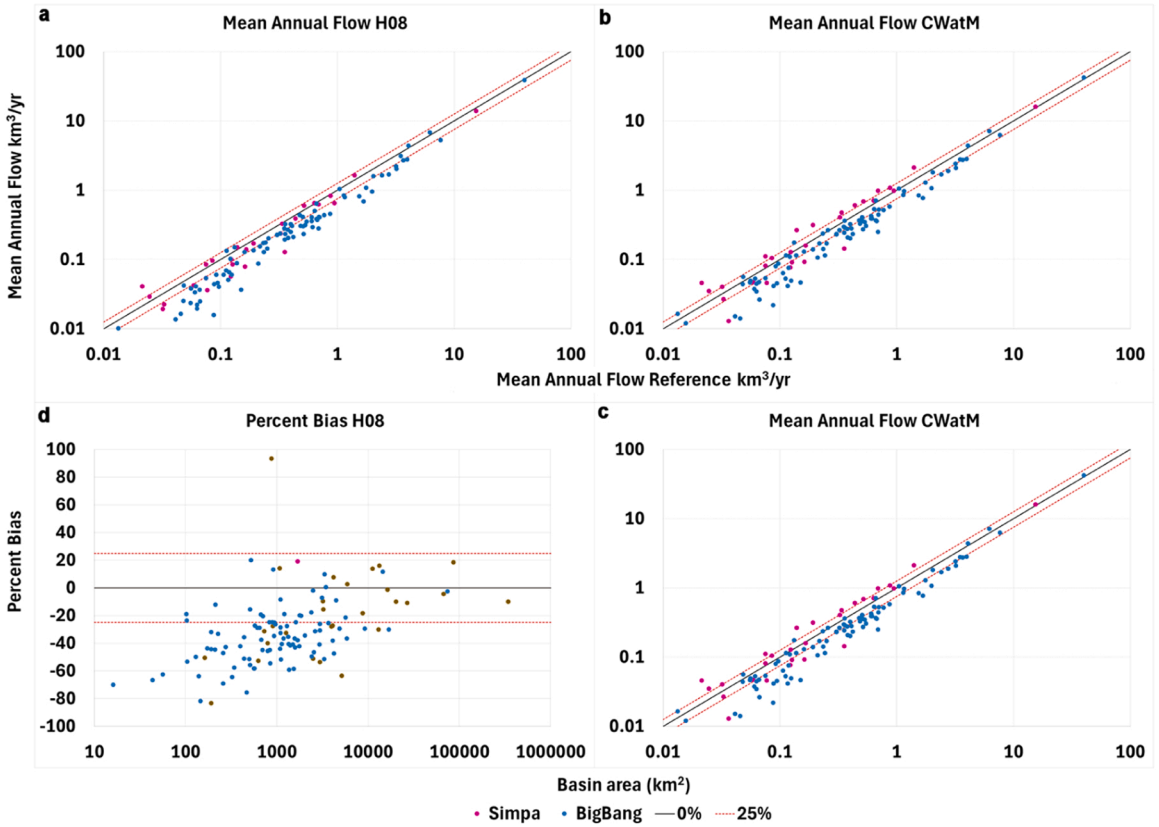

Fig. 3. a: Scatterplot of mean annual flows produced by the H08 model and the local validation models. b: Scatterplot of mean annual flows produced by the CWatM model and the local validation models. c: Scatterplot of percentage bias produced by the H08 model compared to the local validation models as a function of basin area. d: Scatterplot of percentage bias produced by the CWatM model compared to the local validation models as a function of basin area.

prospective analyses, with CWatM offering the best agreement with local data in terms of both accuracy and reliability.

3.2. Flow and potential water availability in different climate scenarios

After validating the performance of the global hydrological models H08 and CWatM, their outputs were used to estimate water flows and compute the potential water availability in the Mediterranean basins under a range of climate scenarios aligned with the

Table 4
Average mean annual flow (km³) in the Mediterranean basin according to model, scenario and period.

Scenario	Values (km³/y)		Change with respect to historical (%)					
	obsclim	historical	ssp126	ssp370	ssp585	ssp126	ssp370	ssp585
Period	80–19	75–14	20–59	20–59	20–59	60–99	60–99	60–99
h08_gswp3	288.39							
h08_gfdl		296.54	2.30	−10.38	−4.39	−6.95	−21.14	−24.40
h08_mri		297.27	−7.39	−9.92	−6.96	−3.48	−19.92	−30.03
h08_ipsl		303.95	−13.82	−20.70	−19.27	−20.14	−33.99	−40.82
h08_mpi		292.10	−13.82	−14.13	−12.29	−7.78	−29.01	−30.56
h08_ukesm1		307.65	−6.64	−16.71	−17.22	−10.94	−33.22	−32.07
mean h08	288.39	299.50	−7.88	−14.41	−12.10	−9.92	−27.52	−31.63
cwatm_gswp3	346.40							
cwatm_gfdl		353.54	5.87	−4.23	−0.53	−2.85	−13.67	−16.16
cwatm_mri		349.98	−0.87	−2.80	−0.31	1.38	−9.75	−19.79
cwatm_ipsl		353.54	−8.31	−11.19	−12.66	−12.75	−22.06	−29.45
cwatm_mpi		353.27	−10.00	−9.64	−8.36	−4.78	−21.76	−23.14
cwatm_ukesm1		351.88	2.57	−2.60	−7.78	−1.17	−15.86	−18.40
mean cwatm	346.40	352.44	−2.15	−6.10	−5.93	−4.05	−16.63	−21.40

IPCC AR6 framework. The results are organized by hydrological model, climate scenario (namely *obsclim*, *historical*, *ssp126*, *ssp370* and *ssp585*) and by the corresponding time windows of analysis (1980–2019, 1975–2014, 2020–2059 and 2060–2099).

Table 4 presents the simulated average annual water flows across the Mediterranean basins. The table shows mean annual flows for the *obsclim* and *historical* scenarios and percentage changes with respect to *historical* for future scenarios. For the *obsclim* scenario, which is based on reanalysis data and represents recent historical conditions, a single value is provided for each hydrological model. In contrast, for the scenarios derived from climate model projections (*historical*, *ssp126*, *ssp370* and *ssp585*), five values are shown per model, corresponding to the different global climate models used as forcings in the ISIMIP3b framework. This structure enables the assessment of inter-model variability and highlights the uncertainty linked to both greenhouse gas emission pathways and differences in climate model formulations.

Both models indicate a general trend of declining water flows as emission levels increase and projections move toward the end of the century. The most pronounced reductions occur under the SSP5–8.5 high-emissions scenario, particularly in the 2060–2099 period. Additionally, a wider spread among climate model projections is observed under the higher emissions scenarios, reflecting greater uncertainty in future hydrological conditions as the impacts of climate change intensify. CWatM generally simulates higher runoff values than H08 across the Mediterranean region. Under the *obsclim* scenario, H08 estimates a mean annual flow of 288.39 km^3 /year, while CWatM projects 346.40 km^3 /year, representing a discrepancy of approximately 20 %. This variation reflects the influence of model structure and calibration on runoff estimation and highlights the uncertainty inherent to global hydrological simulations. Although no consistent observational dataset of natural flows exists for the Mediterranean region to determine which model provides a more accurate representation, both models exhibit similar spatial distributions and interannual trends. Partial comparisons with regional models indicate that CWatM performs slightly better in the Ebro basin, while H08 provides a closer match in the Po basin. To reduce model-specific biases, the results presented in this study are based on the mean of both models, which offers a more balanced and representative estimate of large-scale runoff behavior.

For the historical scenario, averaged across the five climate model forcings, H08 yields 299.50 km^3 /year compared to 352.44 km^3 /year from CWatM. Both ISIMIP3b models project a significant decline in mean annual flows over the 21st century. The H08 model, which provides lower baseline runoff estimates, also suggests steeper reductions, ranging from 7.88 % to 14.41 % for the mid-century period (2020–2059), and from 9.92 % to 31.63 % for the late-century period (2060–2099), depending on the emissions scenario. In contrast, the reductions projected by CWatM are more moderate, ranging from 2.15 % to 6.10 % in the mid-century and from 4.05 % to 21.40 % by the end of the century.

Table 5 presents the mean annual runoff simulated in the representative Mediterranean basins with a contributing area greater than 14,000 km^2. The values shown correspond to the average outputs of both global hydrological models (H08 and CWatM), calculated over all available climate forcings for each scenario within the ISIMIP3b framework. This table provides a comparative overview of projected mean annual flow at the basin scale, facilitating the analysis of spatial patterns and model consistency.

Table 5
Average mean annual flow (km^3) in the main basins in the study area according to model, scenario and period.

Basin	Value (km^3/y)		Change with respect to historical (%)					
	obsclim	historical	ssp126	ssp370	ssp585	ssp126	ssp370	ssp585
	80–19	75–14	20–59	20–59	20–59	60–99	60–99	60–99
Rhone	54.30	55.47	−8.02	−8.98	−7.10	−4.04	−16.20	−16.29
Ebro	14.60	14.77	−9.39	−16.38	−14.31	−8.59	−23.69	−29.06
Po	41.83	41.50	−4.23	−6.07	−4.32	−2.76	−10.30	−15.87
Moulouya	2.53	2.48	−10.97	−21.41	−28.05	−26.19	−44.45	−53.90
Maritsa	8.42	9.24	−2.96	−7.29	−10.40	−13.14	−29.30	−34.22
Bayy al Kabir	0.43	0.41	15.19	14.36	4.22	6.71	5.28	13.32
Cheliff	2.57	2.88	−13.86	−19.82	−23.77	−25.07	−45.37	−54.81
Dufan	1.04	0.99	5.48	2.60	−7.29	−5.74	−8.86	−12.96
Qurayn	0.36	0.35	20.28	10.46	−5.92	1.57	0.22	−0.46
Vardar	3.50	3.80	−3.48	−12.55	−8.56	−13.27	−31.17	−38.37
Menderes	5.09	5.44	−9.07	−18.47	−18.19	−14.44	−40.68	−44.43
Capraz	5.01	5.28	−5.23	−10.76	−11.07	−9.45	−33.38	−33.16
El Arish	0.13	0.13	6.20	−4.62	−9.62	−6.04	−19.18	−17.16
Orontes	5.23	5.33	−4.42	−9.74	−10.15	−4.78	−31.80	−33.56
Medjerda	3.43	3.91	−9.02	−12.84	−14.86	−14.63	−29.92	−34.82
Jucar	1.81	1.89	−3.08	−15.36	−13.71	−18.23	−28.45	−37.71
Cayhan	5.14	5.28	−4.16	−10.91	−10.24	−6.23	−33.49	−33.52
Seyhan	3.58	3.76	−4.83	−13.35	−11.78	−7.97	−34.61	−34.96
Bojana	11.04	11.18	−1.12	−7.34	−4.79	−4.94	−18.03	−22.69
Strymon	2.03	2.25	−4.67	−12.35	−9.12	−14.83	−31.95	−39.30
Gediz	3.08	3.21	−11.48	−18.15	−17.91	−15.91	−41.66	−45.80
Tiber	5.88	5.97	1.81	−9.47	−6.79	−2.36	−20.08	−27.92
Segura	0.92	0.99	−2.43	−12.78	−15.77	−15.81	−31.08	−39.74
El Brega	1.02	1.00	−5.07	−8.22	−8.74	−13.59	−15.28	−19.28
Halk el Menzel	0.69	0.79	−13.86	−17.52	−18.30	−19.95	−30.87	−36.13
La Macta	0.50	0.59	−20.03	−30.51	−31.08	−32.75	−53.69	−62.15
Adige	7.01	7.04	−0.26	−2.66	1.04	2.36	−7.91	−13.49

The results reveal considerable variability in mean annual runoff across the Mediterranean basins. The Rhône basin, which also has the largest contributing area, registers the highest mean annual flow, followed by the Po basin. Five basins: Rhône, Po, Bojana, Tiber, and Adige, can be classified as humid, with mean annual runoff exceeding 350 mm/year. Eleven basins fall within an intermediate range, with runoff between 100 mm/year and 350 mm/year, while twelve basins are considered arid, exhibiting mean annual runoff below 100 mm/year. Although the two global hydrological models provide consistent spatial patterns of runoff, their mean annual estimates differ by approximately 18 % on average, with CWatM generally producing higher runoff values than H08. This difference is more pronounced in arid basins (runoff < 100 mm) and tends to diminish in humid areas (runoff > 350 mm). Projected changes in runoff also vary significantly across basins. Some basins, such as the Moulouya, Cheliff, and La Macta, exhibit extreme declines, with reductions exceeding 50 % in mean annual runoff under the high-emissions scenario (SSP5–8.5) for the late-century period (2060–2099). These spatial disparities underscore the uneven impacts of climate change on water availability in the region.

Table 6 presents the values of potential water availability estimated by the WAAPA model, based on simulated flows and incorporating the reservoir management and operational conditions described in the methodology. The results presented below describe the availability of surface water resources only. Although groundwater constitutes a crucial component of total water supply in many Mediterranean basins, particularly in areas with limited surface runoff, it has not been included in this analysis. The implications of this limitation are further discussed in Section 4.4.

As with the mean annual flow results, the estimates for future scenarios reflect variability across the different climate models. Despite notable differences in mean annual flow projections between the two global hydrological models, the estimates of potential water availability are remarkably consistent. Under the *obsclim* scenario, the H08 model yields a potential availability of 84.15 km^3 / year, representing 29.18 % of its simulated mean annual flow, while the CWatM model estimates 87.35 km^3 /year, or 25.22 % of its corresponding runoff. This convergence can be explained by two main factors. First, in many basins the available volume is determined primarily by the storage capacity of reservoirs rather than by the mean hydrological regime. Under annual regulation, the available resource approximates the sum of the active storage capacity and the guaranteed minimum flow, which reduces the sensitivity to differences in simulated runoff. Second, water availability is governed more by the frequency of low-flow events and the temporal variability of discharge than by its mean value. For instance, under natural flow conditions (i.e., without reservoir regulation), the H08 model estimates higher water availability than CWatM despite producing lower mean runoff, a result that is further discussed in Section 4.1. These findings highlight that indicators based on supply reliability provide a more consistent measure of water scarcity than mean annual runoff alone.

For the historical scenario, averaged across the five climate drivers, potential availability is estimated at 87.85 km^3 /year for H08 and 89.14 km^3 /year for CWatM. The projected reduction in water availability is consistently greater than the reduction in mean annual flow, highlighting the compounding effect of reservoir management and supply constraints under drier conditions. Despite differences in runoff estimates, both global hydrological models produce very similar projections of potential availability. For the H08 model, the estimated reductions range from 13.22 % to 20.60 % in the short-term time window (2020–2059) and from 13.96 % to 42.30 % in the long-term window (2060–2099). The CWatM model projects comparable declines, ranging from 13.98 % to 19.16 % in the short term and from 13.99 % to 39.81 % in the long term.

Table 7 presents the estimated values of potential water availability in the representative Mediterranean basins with contributing areas larger than 14,000 km^2. These values were obtained by averaging the results from the two global hydrological models (H08 and CWatM) across all available climate forcings within each scenario. H08 yields higher availability in 11 basins and CWatM in 17. The figures reflect the combined influence of projected runoff, local hydrological characteristics, and reservoir operating conditions, providing a basin-scale perspective on future water supply capacity under changing climate conditions.

The results presented in the table reveal substantial spatial disparities in potential water availability across Mediterranean basins. While the average availability for the entire region is approximately 27 % of the mean annual flow, individual basins display markedly higher or lower values. Four basins: Ebro, Júcar, Ceyhan, and Seyhan, exhibit availability ratios exceeding 50 % of their mean annual

Table 6
Potential water availability (km^3) in the Mediterranean basin according to model, scenario and period.

Scenario	Values (km^3/y)		Change with respect to historical (%)					
	obsclim	historical	ssp126	ssp370	ssp585	ssp126	ssp370	ssp585
Period	80–19	75–14	20–59	20–59	20–59	60–99	60–99	60–99
h08_gswp3	84.15							
h08_gfdl		91.22	−8.10	−19.71	−15.84	−13.90	−30.23	−34.04
h08_mri		89.00	−14.68	−13.75	−17.08	−10.56	−30.82	−39.85
h08_ipsl		90.44	−18.47	−22.72	−23.10	−23.28	−39.89	−50.38
h08_mpi		82.69	−14.06	−19.03	−18.53	−9.78	−35.40	−44.40
h08_ukesm1		85.91	−10.82	−20.21	−28.66	−11.77	−41.44	−43.10
mean h08	84.15	87.85	−13.22	−19.09	−20.60	−13.96	−35.50	−42.30
cwatm_gswp3	87.35							
cwatm_gfdl		90.84	−4.12	−17.50	−11.51	−14.05	−28.85	−31.54
cwatm_mri		84.69	−10.08	−4.80	−7.24	−3.20	−20.94	−31.47
cwatm_ipsl		90.84	−18.76	−20.76	−22.44	−24.33	−38.19	−47.84
cwatm_mpi		89.78	−20.97	−20.67	−22.78	−12.45	−35.81	−44.59
cwatm_ukesm1		89.56	−15.82	−19.71	−31.22	−15.20	−38.53	−43.12
mean cwatm	87.35	89.14	−13.98	−16.83	−19.16	−13.99	−32.60	−39.81

Table 7
Potential water availability (km³) in the main basins in the study area according to model, scenario and period.

Basin	Value (km³/y)		Change with respect to historical (%)					
	obsclim	historical	ssp126	ssp370	ssp585	ssp126	ssp370	ssp585
	80–19	75–14	20–59	20–59	20–59	60–99	60–99	60–99
Rhone	14.30	14.80	−17.71	−18.42	−18.13	−13.33	−29.91	−34.91
Ebro	8.69	8.60	−9.84	−13.32	−13.45	−7.57	−23.38	−33.18
Po	11.09	11.66	−24.04	−21.31	−26.08	−18.71	−37.18	−48.27
Moulouya	0.43	0.44	−14.16	−19.28	−32.18	−29.06	−45.05	−53.36
Maritsa	2.33	2.56	−12.24	−18.94	−26.62	−18.33	−43.39	−47.65
Bayy al Kabir	0.08	0.07	7.31	4.44	8.88	4.21	−0.30	9.22
Cheliff	0.99	1.04	−9.32	−22.10	−26.99	−22.15	−40.69	−51.81
Dufan	0.15	0.13	2.11	1.32	−2.92	−0.23	−5.59	−6.67
Qurayn	0.05	0.05	7.95	8.90	5.22	9.06	2.25	6.05
Vardar	1.16	1.39	−10.29	−21.95	−20.87	−11.25	−37.66	−46.77
Menderes	2.29	2.49	−14.87	−24.78	−22.57	−14.81	−43.62	−41.87
Capraz	1.63	1.70	−4.37	−19.73	−16.38	−9.60	−41.17	−36.96
El Arish	0.02	0.02	13.79	−1.22	−16.73	2.39	−14.94	−13.91
Orontes	0.79	0.80	−13.86	−15.28	−21.20	−15.26	−38.80	−39.26
Medjerda	1.69	1.84	−7.42	−18.73	−17.47	−20.94	−34.57	−42.05
Jucar	1.17	1.09	−7.91	−14.61	−15.93	−15.62	−26.59	−39.61
Cayhan	3.15	2.99	−12.07	−10.54	−19.19	−11.83	−35.78	−34.70
Seyhan	2.09	2.11	−14.02	−15.25	−20.56	−12.48	−36.85	−35.48
Bojana	1.10	1.16	−12.44	−19.21	−18.76	−14.69	−34.33	−41.45
Strymon	0.43	0.46	−8.49	−20.02	−24.99	−16.43	−42.50	−49.90
Gediz	1.11	1.33	−14.40	−28.65	−22.25	−13.91	−47.34	−43.84
Tiber	0.86	0.90	−7.04	−16.20	−19.96	−10.09	−31.66	−52.22
Segura	0.45	0.42	−7.42	−14.07	−15.48	−10.97	−28.35	−42.31
El Brega	0.13	0.12	−6.38	−10.71	−8.11	−8.90	−11.31	−16.44
Halk el Menzel	0.29	0.28	−10.77	−15.16	−13.63	−15.39	−36.54	−39.14
La Macta	0.22	0.23	−22.15	−30.25	−32.53	−26.73	−51.04	−57.63
Adige	2.00	1.89	−22.57	−21.33	−25.73	−19.58	−41.64	−54.60

flow, a reflection of their substantial reservoir storage relative to natural inflows. In contrast, the Bojana basin shows values below 10 %, primarily due to limited storage capacity and highly irregular hydrological regimes. Interestingly, other basins such as the Adige, despite lacking major storage infrastructure, achieve water availability levels around 30 %, thanks to more stable flow patterns. Projected changes in potential water availability broadly follow the trends in runoff reduction but also exhibit significant variability among basins. Notably, the Moulouya, Cheliff, Tiber and La Macta basins are projected to experience reductions exceeding 50 % under the SSP5–8.5 scenario for the 2060–2099 period.

The results for potential water availability reinforce the trends identified in runoff projections, indicating a progressive decline in

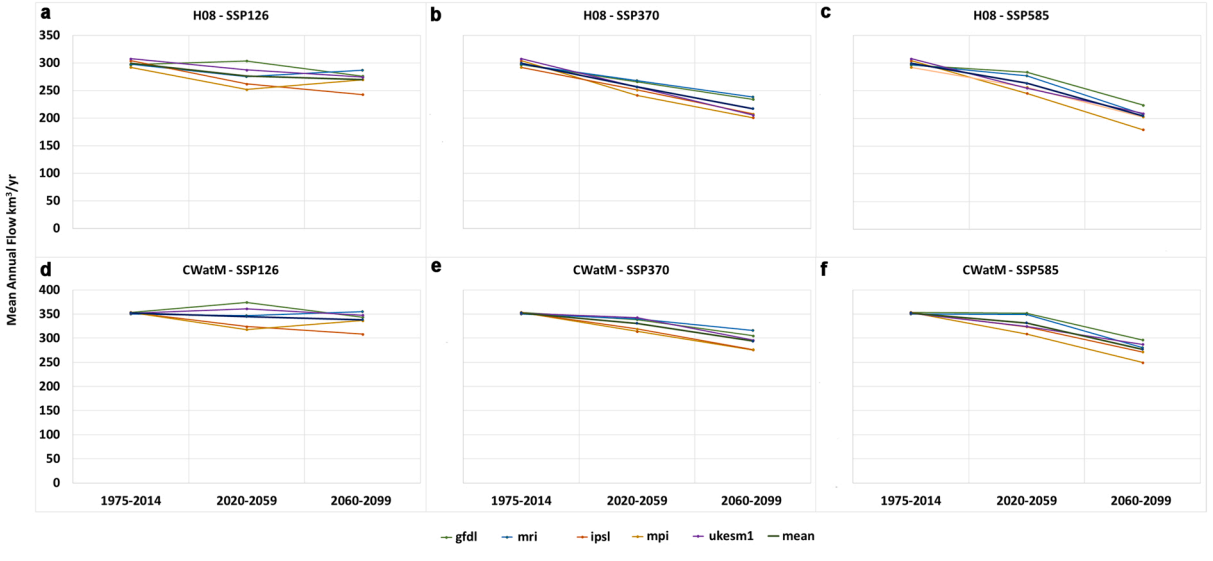

Fig. 4. Evolution of mean annual flow in the different climate scenarios analyzed. a: H08 model, SSP1–2.6. b: H08 model, SSP3–7.0. c: H08 model, SSP5–8.5. d: CWatM model, SSP1–2.6. f: CWatM model, SSP3–7.0. f: CWatM model, SSP5–8.5.

the volume of water potentially available for consumptive uses across Mediterranean basins. This reduction is particularly pronounced under high-emission scenarios and towards the end of the century. While both hydrological models (H08 and CWatM) show consistent trends, CWatM tends to estimate slightly lower levels of potential water availability than H08, in contrast to its generally higher runoff projections, suggesting greater variability in its outputs. Overall, the tables presented offer a robust quantitative overview of future water resource dynamics in the Mediterranean and provide a foundation for analyzing their spatial distribution and temporal evolution in greater detail.

3.3. Temporal evolution of flow and potential water availability

The evolution of mean annual flow and potential water availability in the Mediterranean basins throughout the 21st century is illustrated in Figs. 4–6, with distinctions made by climate scenario and time period.

Fig. 4 specifically depicts the temporal evolution of mean annual runoff in the Mediterranean basins, as simulated by the two global hydrological models (H08 and CWatM) across the three emission scenarios analyzed (SSP1–2.6, SSP3–7.0, and SSP5–8.5). The figure includes historical results for the period 1975–2014, as well as projections for the near term (2020–2059) and long term (2060–2099). The top row of graphs corresponds to H08, while the bottom row displays results from CWatM. Each panel shows the outputs of the five climate forcings used in ISIMIP3b, along with their multi-model average. Figure S3 shows the same information, but representing percentage changes of mean annual flow with respect to the *historical* scenario. The figures clearly illustrate a downward trend in average annual runoff as emissions intensify and the century progresses. This decline is most pronounced in the SSP5–8.5 scenario for the 2060–2099 period, where reductions in runoff approach 30 % compared to the historical baseline.

Fig. 5 illustrates the projected evolution of potential water availability in the Mediterranean basins, using the same structure and format as Fig. 4. Results are presented for the historical period (1975–2014) and the two future time horizons (2020–2059 and 2060–2099), across the three emission scenarios (SSP1–2.6, SSP3–7.0, and SSP5–8.5). As in the previous figure, the top row corresponds to the H08 model and the bottom row to CWatM, with individual projections shown alongside their multi-model average. Figure S4 shows the same information, but representing percentage changes of water availability with respect to the *historical* scenario. The evolution of potential water availability generally mirrors the trends observed in mean annual flow, showing a progressive decline under more severe emission scenarios and towards the end of the century. However, the magnitude of the reduction and its spatial distribution vary across regions, particularly in basins with limited storage capacity and more irregular flow regimes. In the most pessimistic scenario (SSP5–8.5), the projected loss of potential water availability by 2060–2099 exceeds 30 % relative to the historical period. Both Figs. 4 and 5 highlight that, despite the natural dispersion between climate projections, the overall trends remain consistent across models within each scenario, reinforcing the robustness of the results.

Finally, Fig. 6 provides a synthesis of the results for the entire Mediterranean region. The panels on the left show the evolution of mean annual flow, while those on the right correspond to potential water availability. The upper row presents absolute values (in km^3/year), and the lower row shows the relative changes (%) compared to the historical period (1975–2014). To highlight robust system-level trends, the figure displays the multi-model mean calculated from the five global climate models used as forcings. As observed in previous figures, CWatM produces higher estimates of mean annual flow than H08 during the historical period. However, the estimates of potential water availability are much more aligned between the two models, suggesting that differences in runoff generation translate less directly into differences in regulated water availability. The disparity between the models is therefore more pronounced

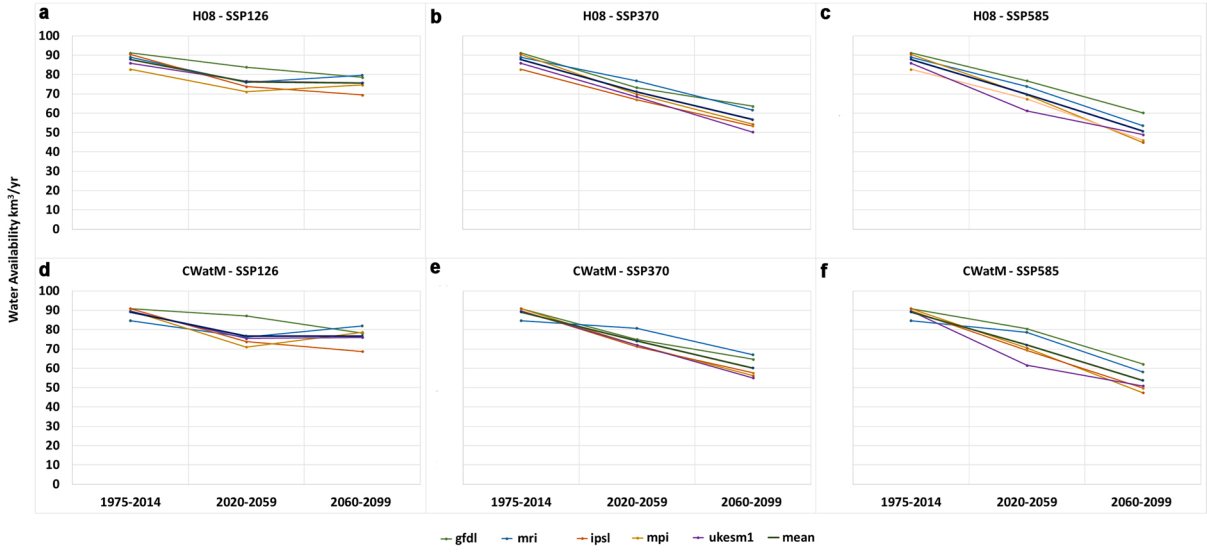

Fig. 5. Evolution of potential water availability in the different climate scenarios analyzed. a: H08 model, SSP1–2.6. b: H08 model, SSP3–7.0. c: H08 model, SSP5–8.5. d: CWatM model, SSP1–2.6. f: CWatM model, SSP3–7.0. f: CWatM model, SSP5–8.5.

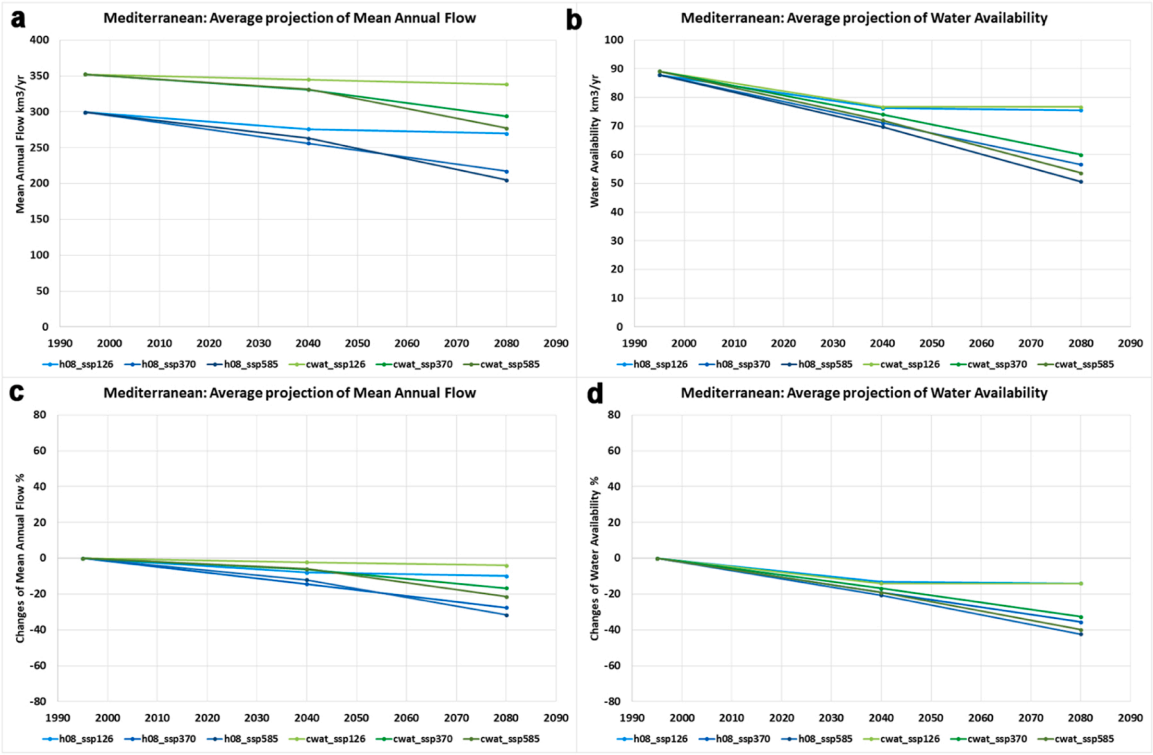

Fig. 6. Average evolution of the mean annual flow and potential water availability for the two hydrological models in the different climate scenarios analyzed. a: Absolute values, mean annual flow. b: Absolute values, potential water availability. c: Relative values, mean annual flow. d: Relative values, potential water availability.

for total flow than for potential availability. Both models exhibit similar temporal trends across the three emission scenarios (SSP1–2.6, SSP3–7.0, and SSP5–8.5), showing a progressive decline in both indicators over time. In the near-term horizon (2020–2059), the reduction in mean annual flow ranges between 2 % and 12 %, while the decline in potential water availability is more pronounced, between 13 % and 21 %. In the long-term horizon (2060–2099), projected reductions intensify, with losses in flow ranging from 5 % to 32 %, and in availability from 14 % to 42 %. These results underscore the growing impact of climate change over time, particularly on the volume of water that can be effectively stored and used.

3.4. Spatial analysis of the results

To support spatial analysis of the results, high-resolution thematic maps were created to depict key variables along the river network of Mediterranean basins. These maps enable the identification of distinct spatial patterns across the different scenarios analyzed. First, static variables related to pressures on water resources are presented. Figure S5 illustrates the spatial distribution of these pressures: the upper panel displays population density (inhabitants/km^2), while the lower panel shows irrigation density (hectares/km^2). Overall, population density remains low across most of the region, with higher concentrations surrounding major urban centers. In contrast, the highest irrigation densities are found primarily in the Ebro River and Po River valleys, which receive runoff from the Pyrenees and the Alps, respectively. This spatial information allows for a clear linkage between regions of greatest vulnerability and underlying structural and socioeconomic factors affecting water resources.

Fig. 7 illustrates the spatial distribution of cumulative reservoir capacity and potential water availability along the river network of the Mediterranean basins under the *obsclim* scenario. At each point along the rivers, the values represent the total upstream sum, either of reservoir storage capacity or potential water availability. For potential water availability, the figure shows the average of results obtained from the H08 and CWatM models for the *obsclim* scenario, reflecting conditions during the period 1980–2019. To enable meaningful comparisons across different areas, both reservoir capacity and potential water availability are expressed as percentages of the average annual flow at each location, also averaged between the two hydrological models. The total regulated reservoir capacity included in the model is 67.64 km^3 , which corresponds to 21.3 % of the average annual flow of 317.40 km^3 /year. Potential water availability amounts to 85.75 km^3 /year, representing 27.0 % of the average annual flow. The figure reveals a significant spatial correlation between reservoir capacity and potential water availability, highlighting that water availability is largely governed by the extent of upstream reservoir storage.

The upper panel of Figure S6 analyzes the relationship between average annual flow and potential water availability through scatter plots comparing two scenarios. The left graph shows the average values from the two hydrological models under the *obsclim*

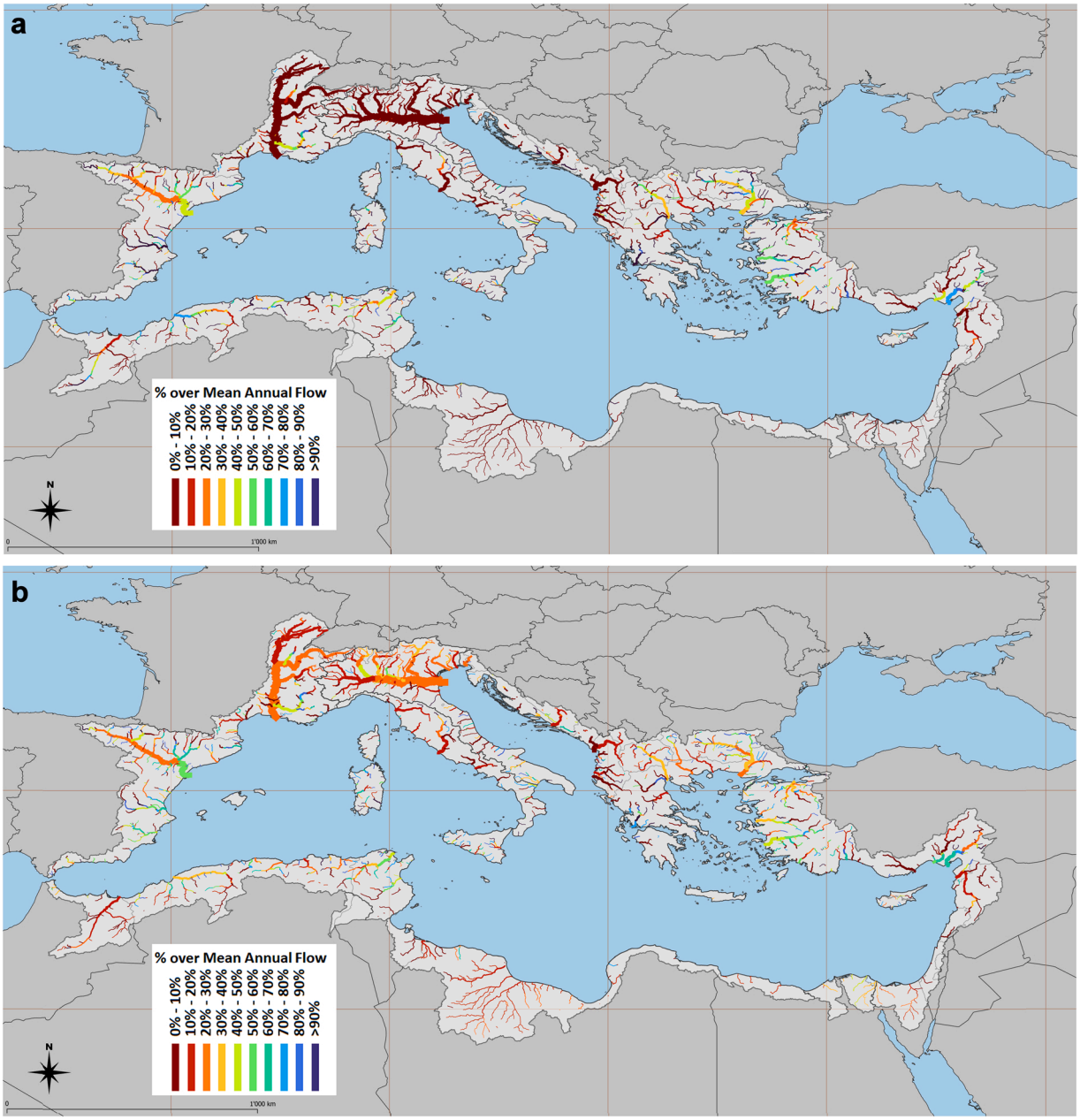

Fig. 7. Reservoir volume (a) and potential water availability in the *obsclim* scenario (b) along the rivers of the Mediterranean basin. Both variables are expressed as a percentage of mean annual flow in the natural regime in the *obsclim* scenario.

scenario, representing the period 1980–2019. The right graph presents the average of all available projections under the SSP5–8.5 scenario for the period 2060–2099. Reference lines indicating potential water availability at 100 %, 75 %, 50 %, and 25 % of the average annual flow are included for easier interpretation. Each point represents a basin within the model. The plots reveal a wide range of behaviors that reflect local hydrological variability and reservoir capacity. Basins with larger reservoir volumes tend to regulate a higher percentage of their average annual flow, whereas basins lacking reservoirs or located in regions with highly irregular hydrology exhibit much lower percentages of regulated flow. Notably, the scatter in the SSP5–8.5 scenario is more pronounced than in the current conditions, suggesting increased hydrological variability under future climate change.

Maps showing the relative changes in average annual flow and potential water availability for each future scenario were developed with reference to the historical period. Fig. 8 illustrates the results for the SSP5–8.5 scenario in the 2060–2099 time window. The values represent the average of the outputs from the two hydrological models (H08 and CWatM) forced by the five global climate models used. Under this high-emission scenario, the average annual flow is projected to decrease by 26.10 %, which reflects the mean

of a 31.63 % reduction estimated by the H08 model and a 21.40 % reduction estimated by the CWatM model. Uncertainty is notable, with reductions ranging from 24.40 % to 40.82 % across climate models for H08, and from 16.16 % to 29.95 % for CWatM. The decline in potential water availability is even more pronounced than that of flow. The projected average reduction is 41.05 %, based on a 42.30 % decrease estimated by H08 and 39.81 % by CWatM. The variability across climate models spans from 34.04 % to 50.38 % for H08, and from 31.47 % to 47.84 % for CWatM.

The lower panel of Figure S6 illustrates the relationship between historical and future values of the variables analyzed for the 363 basins included in the model. The comparison is made between the historical scenario (1975–2014) and the SSP5–8.5 scenario for the period 2060–2099. The graph on the left shows mean annual flow, while the graph on the right displays potential water availability. Reference lines corresponding to 100 %, 75 %, 50 %, and 25 % of the historical values are included to guide interpretation. As shown, the variability in mean annual flow is lower than that observed in potential water availability. For mean annual flow, 55 % of the basins fall within the 25–50 % reduction band, 40 % show a reduction of less than 25 %, and only 5 % experience a decrease exceeding

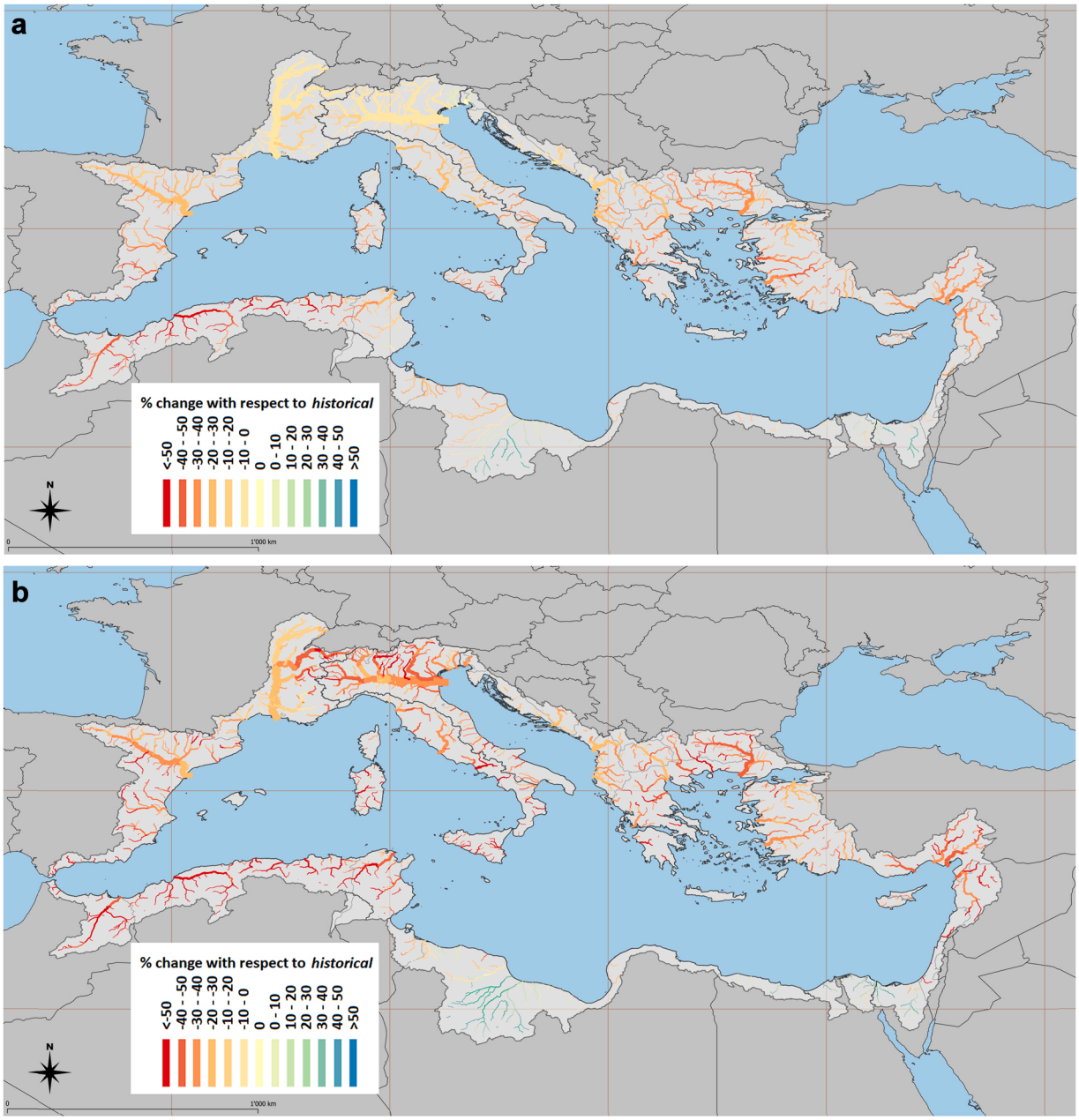

Fig. 8. Changes in mean annual flow (a) and potential water availability (b) in the SSP5–8.5 scenario and the period 2060–2099, expressed as a percentage in relation to the historical scenario and the period 1975–2014.

50 %, though none drop below 25 % of their historical value. In contrast, the distribution of potential water availability is more dispersed. Approximately 48 % of basins fall within the 25–50 % reduction band, 26 % show reductions below 25 %, and 25 % experience losses greater than 50 %, including 8 basins (2 %) where the reduction exceeds 75 % of historical levels. This increased variability is largely attributable to the growing impact of hydrological variability on reservoir regulation capacity, as discussed in detail in the corresponding section.

4. Discussion

The discussion of the results is organized around three key dimensions that influence the future availability of water resources in Mediterranean basins: (1) the role of reservoir storage capacity in shaping potential water availability; (2) the impact of increasing hydrological variability on the reliability of water supply; and (3) the comparison between projected potential water availability and spatial indicators of water demand, to identify regions at risk of future water management challenges.

4.1. The role of storage capacity in water availability

One of the key factors influencing potential water availability in Mediterranean basins is the presence of a highly developed system of reservoirs. This infrastructure plays a critical role in regulating the naturally variable hydrological regime, enabling the redistribution of water resources across both space and time. By mitigating the effects of seasonality and extreme hydrological events, reservoirs help to stabilize supply and support more consistent water availability. The results indicate that, even under scenarios of reduced inflows, basins with greater reservoir storage capacity tend to maintain comparatively higher levels of water availability. This highlights the strategic importance of reservoir infrastructure as an essential adaptation measure to climate change. At the same time, it underscores the need to ensure the efficient and flexible operation of these systems under increasingly demanding supply and demand conditions.

The influence of reservoir storage capacity on potential water availability becomes particularly evident when comparing results from the WAAPA model under two different configurations: one that includes existing regulation capacity, and another that assumes no storage infrastructure. Table 8 presents the potential water availability values that would be expected in the absence of reservoir regulation across the Mediterranean basins.

Under reference conditions (*obsclim* scenario), the average annual potential water availability in the Mediterranean basin without considering reservoir storage is estimated at 40.00 km^3 /year, based on the average of values provided by the global hydrological models H08 (44.08 km^3/year) and CWatM (35.91 km^3/year). When reservoir storage capacity is included, this figure increases sharply to 85.75 km^3 /year, representing 214 % of the value without regulation. In other words, 53 % of the current potential water availability in the basin is attributable to the buffering and redistribution capacity provided by reservoirs. The results by model reveal notable differences: with storage considered, the H08 model estimates availability at 84.15 km^3 /year, an increase of 191 % over the unregulated scenario, while CWatM estimates 87.35 km^3 /year, corresponding to a 243 % increase. These differences become even more pronounced under the most severe climate projection (SSP5–8.5, period 2060–2099), where average increases reach 252 %, with H08 projecting a 207 % increase and CWatM a 318 % increase.

Fig 9 further explores the relationship between reservoir storage capacity and potential water availability under the *obsclim* scenario. The left panel presents a scatter plot showing the correlation between cumulative reservoir storage and potential water availability in each basin, both expressed as a percentage of mean annual flow. The plot clearly illustrates how storage capacity enhances the capacity to regulate and mobilize water resources. The right panel displays a scatter plot comparing potential water availability without reservoirs to that with reservoirs. Each point represents one of the 363 modeled basins. Diagonal reference lines mark increases of 250 %, 500 %, and 1000 % in availability due to reservoir regulation. The analysis shows that 126 basins lack

Table 8
Potential water availability (km^3) in the Mediterranean basin excluding reservoirs, according to model, scenario and time horizon.

Scenario	Values km^3/y		Change with respect to historical (%)					
	obsclim	historical	ssp126	ssp370	ssp585	ssp126	ssp370	ssp585
Period	80–19	75–14	20–59	20–59	20–59	60–99	60–99	60–99
h08_gswp3	44.08							
h08_gfdl		49.32	−10.63	−22.35	−15.63	−18.03	−34.43	−37.32
h08_mri		47.65	−17.92	−14.58	−18.21	−11.03	−29.70	−43.49
h08_ipsl		48.50	−22.92	−24.74	−26.37	−24.45	−44.51	−55.42
h08_mpi		43.61	−17.08	−21.72	−25.43	−10.44	−38.55	−51.76
h08_ukesm1		46.91	−18.16	−29.06	−38.99	−16.38	−49.80	−52.81
mean h08	44.08	47.20	−17.32	−22.49	−24.81	−16.20	−39.36	−48.03
cwatm_gswp3	35.91							
cwatm_gfdl		37.89	−7.47	−26.11	−9.49	−26.37	−38.41	−41.50
cwatm_mri		35.41	−19.05	−7.77	−11.03	−9.69	−23.81	−43.46
cwatm_ipsl		37.89	−30.02	−30.48	−32.76	−32.85	−53.34	−64.07
cwatm_mpi		38.15	−32.77	−30.14	−39.82	−16.93	−49.67	−61.51
cwatm_ukesm1		37.48	−31.66	−33.81	−50.14	−26.36	−58.28	−63.22
mean cwatm	35.91	37.36	−24.26	−25.89	−28.85	−22.59	−44.96	−54.89

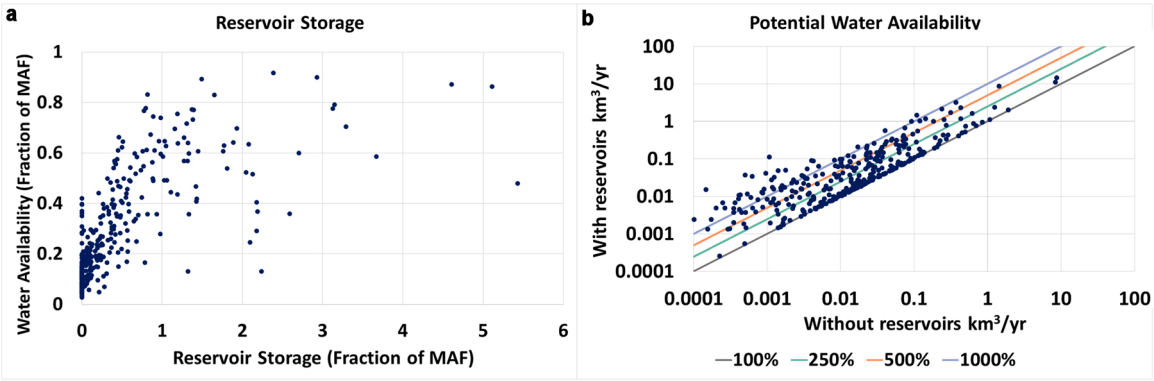

Fig. 9. a: Relationship between reservoir storage and potential water availability in the *obsclim* scenario. b: Relationship between potential water availability without reservoirs and with reservoirs in the *obsclim* scenario.

significant storage capacity for flow regulation. Among the 237 basins with regulation, 41 % see increases in potential availability of less than 250 %; 24 % experience increases between 250 % and 500 %; and 19 % achieve increases between 500 % and 1000 %. Notably, in 39 basins (16 %), regulation results in a tenfold or greater increase in potential water availability. These figures illustrate the transformative role of storage infrastructure, particularly in basins affected by strong seasonality and high hydrological variability. Without the regulation provided by reservoirs, the capacity of the system to meet consumptive water demands, especially during dry years and peak summer periods, would be severely constrained.

The pronounced seasonality and interannual variability characteristic of the Mediterranean climate magnify the importance of reservoirs in ensuring the reliability and resilience of water supply. These infrastructures enable the capture of seasonal surpluses and the temporal redistribution of flows, effectively buffering extreme fluctuations in the hydrological regime. In summary, reservoir regulation not only increases average water availability, but also underpins the stability and adaptive capacity of the water system under variable and changing climatic conditions (Granados et al., 2021). These results highlight the strategic importance of integrating existing infrastructure into climate adaptation planning, while also assessing its resilience and performance under scenarios of reduced future flows.

4.2. *The effect of hydrological variability on water availability*

Potential water availability is influenced not only by reductions in average inflows, but also by the frequency and intensity of dry periods. Increased variability directly undermines the reliability of supply, as prolonged low-inflow periods hinder the ability of reservoirs to sustain adequate storage levels. Consequently, water planning must incorporate variability indicators, rather than relying solely on average annual values, to anticipate potential supply failures and enhance system resilience. To assess the expected evolution of hydrological variability in the basin, the coefficient of variation (CV) of annual inflows was analyzed. Table 9 presents the CV values calculated from the H08 and CWatM models for each scenario and time horizon. The table presents the area-weighted mean coefficient of variation computed across all basins in the model domain. The two models yield very similar variability estimates, suggesting that the observed trends are primarily driven by climatic forcing rather than differences in model structure or parameterization.

Table 9
Coefficient of variation of annual streamflow in the Mediterranean basin according to model, scenario and time horizon.

Scenario	Value		Change with respect to historical (%)					
	obsclim	historical	ssp126	ssp126	ssp370	ssp370	ssp585	ssp585
Period	80–19	75–14	20–59	60–99	20–59	60–99	20–59	60–99
h08_gswp3	0.40							
h08_gfdl		0.42	9.89	11.03	1.62	4.49	14.82	20.46
h08_mri		0.45	14.97	8.42	13.96	7.67	33.21	18.08
h08_ipsl		0.46	−6.42	−3.30	−2.54	3.23	26.79	16.94
h08_mpi		0.44	10.24	13.55	19.75	12.37	23.59	23.54
h08_ukesm1		0.47	0.33	6.07	17.90	14.25	18.00	21.43
mean h08	0.40	0.45	5.56	6.99	10.23	8.48	23.36	20.07
cwatm_gswp3	0.42							
cwatm_gfdl		0.43	6.65	7.55	0.55	7.75	19.25	18.45
cwatm_mri		0.46	11.00	7.21	5.71	2.85	25.11	18.46
cwatm_ipsl		0.43	5.69	10.21	6.95	12.08	38.54	33.67
cwatm_mpi		0.47	2.45	15.39	12.64	7.06	15.50	22.44
cwatm_ukesm1		0.46	3.22	7.21	21.20	14.07	17.91	24.34
mean cwatm	0.42	0.45	5.78	9.55	9.56	8.73	23.10	23.40

In the most extreme scenario analyzed: SSP5–8.5 for the period 2060–2099, the coefficient of variation of annual flows increases by 22 % compared to the reference period, indicating a marked intensification of year-to-year hydrological variability. This increased irregularity has a significant impact on potential water availability, particularly in the absence of regulation infrastructure. In this scenario, the average reduction in mean annual flow relative to the historical period is 26.10 %. When reservoir regulation is considered, the corresponding reduction in water availability is 41.05 %, an additional 15 %age points beyond the decline in flow alone. However, without reservoirs, the reduction in potential availability reaches 51.06 %, representing an impact 24 % greater than the decrease in flow, highlighting the disproportionate effect of increased variability on unregulated systems.

These findings demonstrate that amplified variability significantly compromises the performance of unregulated hydrological systems, as demand shortfalls occur more frequently during dry years, even when long-term average inflows are not drastically reduced. By contrast, reservoirs mitigate this risk by enabling the storage of surplus water during wet years and its gradual release during dry periods. This buffering capacity attenuates interannual fluctuations and enhances the overall stability of the water supply system. Thus, reservoirs play a dual role in climate adaptation: not only do they increase average water availability, as shown in the previous section, but they also moderate temporal variability, thereby improving reliability. This combined effect, quantity and stability, underscores the strategic importance of reservoirs in any integrated and climate-resilient water management strategy.

4.3. *Potential water availability in the face of local water pressure*

A particularly valuable perspective for interpreting the results is the analysis of the relationship between potential water availability and estimated water demand at each river node. This comparison allows the identification of areas where water pressure is highest, and therefore most vulnerable to the impacts of climate change. In certain parts of the Mediterranean basins, the estimated potential availability approaches the total demand, suggesting a high degree of resource exploitation and limited flexibility in the face of reduced inflows. Conversely, other regions, characterized by lower relative pressure or greater adaptive capacity, present a wider margin for adjustment. These spatial contrasts highlight the importance of adopting territorially differentiated approaches to water resource management.

To assess the adequacy of water supply in Mediterranean basins, two fundamental indicators of water pressure were calculated: availability per capita and availability per hectare of irrigated land. In the reference scenario (*obsclim*), the mean annual flow is estimated at 317.40 km^3 /year, serving a population of 199.39 million people and an irrigated area of 5.92 million hectares. The results yield an average per capita availability of approximately 1592 m^3 /person/year, which lies just below the widely used

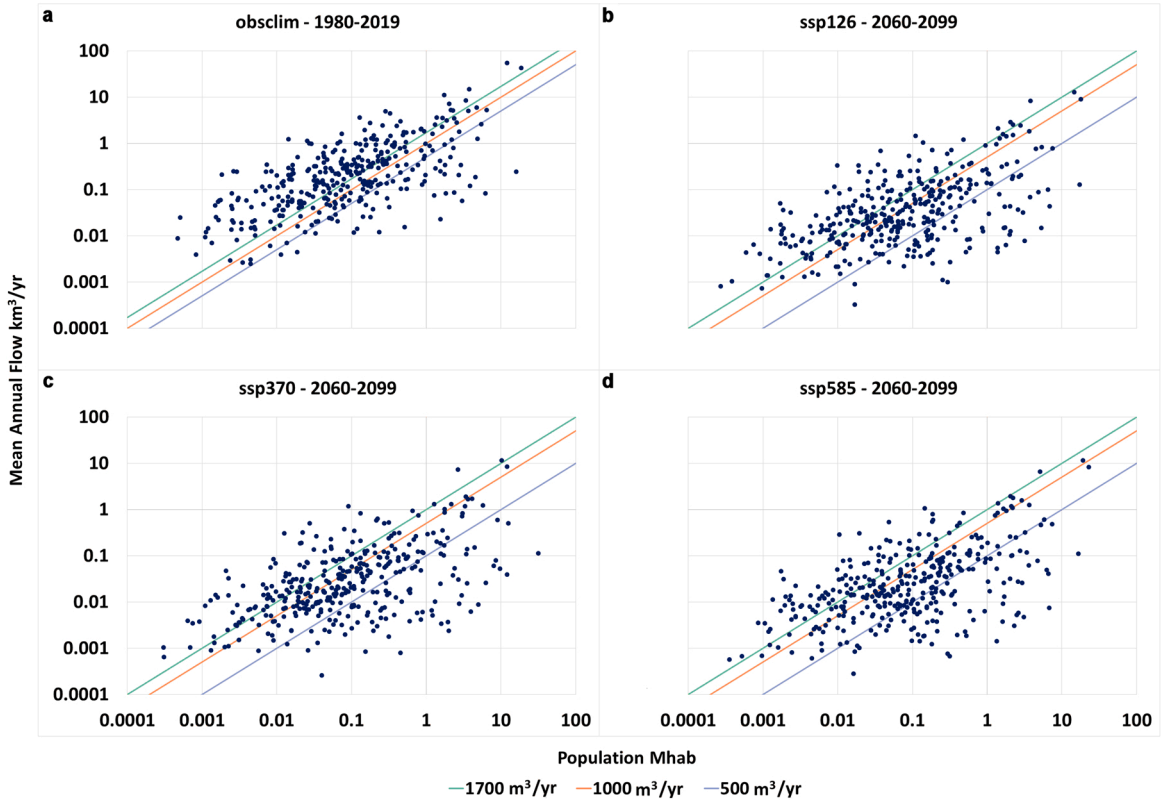

Fig. 10. Relationship between population and renewable water resources. a: *obsclim* scenario. b: SSP1–2.6 scenario in 2060–2099. c: SSP3–7.0 scenario in 2060–2099. d: SSP5–8.5 scenario in 2060–2099.

threshold of 1700 m^3 /person/year proposed by Falkenmark et al. (1989) to indicate water stress. Meanwhile, the average renewable water resources per irrigated hectare is 53,655 m^3 /ha, a figure well above typical crop water requirements (Fader et al., 2016). From this conventional standpoint, the Mediterranean region as a whole appears to maintain an acceptable balance between resource

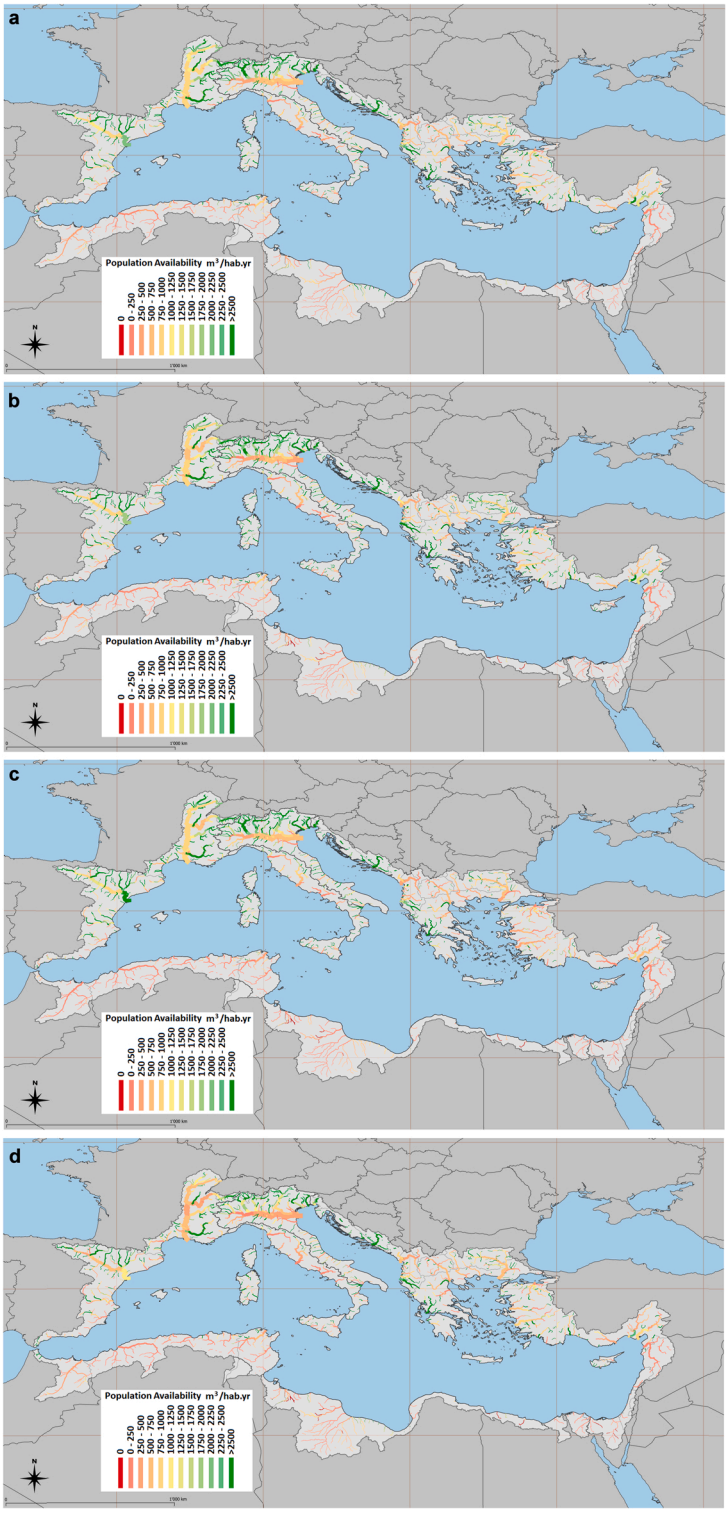

Fig. 11. Spatial distribution of the average per capita water availability in the Mediterranean basin. a: *obsclim* scenario. b: SSP1–2.6 scenario in 2060–2099. c: SSP3–7.0 scenario in 2060–2099. d: SSP5–8.5 scenario in 2060–2099.

availability and demand for both urban supply and irrigation, at least under current mean conditions.

Fig. 10 illustrates the relationship between renewable water resources and population for each modeled basin. The top left panel represents the average values from the two hydrological models (H08 and CWatM) under the *obsclim* scenario for the baseline period 1980–2019. The top right panel shows projections for 2060–2099 under the SSP1–2.6 scenario. The bottom panels correspond to the same future period under SSP3–7.0 and SSP5–8.5, respectively, based on the average of all available climate projections. To contextualize water stress levels, the plots include threshold lines representing per capita water availability of 1700 m^3 , 1000 m^3 and 500 m^3 per person per year, values widely used in the literature to define water stress, relative scarcity, and absolute scarcity, respectively.

The graphs reveal that a substantial number of densely populated basins already experience low levels of water availability, suggesting heightened vulnerability to scarcity, especially under future scenarios of reduced flow. Under current conditions (*obsclim*), 53 basins (14 % of the total) fall below 500 m^3 /person/year, indicating absolute scarcity. An additional 48 basins (13 %) fall within the 500–1000 m^3 /person/year range, and 35 basins (10 %) lie between 1000 and 1700 m^3 /person/year, indicating varying degrees of water stress. In total, 28 % of Mediterranean basins are currently affected by some level of scarcity, encompassing a population of approximately 104 million people, or 52 % of the total basin population (199 million). In the most adverse scenario (SSP3–7.0, 2060–2099), the situation worsens markedly. The number of basins with less than 500 m^3 /person/year rises to 81 (22 %), while 42 basins (12 %) fall between 500 and 1000 m^3 /person/year, and 45 basins (12 %) range between 1000 and 1700 m^3 /person/year. Altogether, 34 % of the basins would experience some form of water scarcity. Importantly, these basins are projected to host 192 million people, or 73 % of the 262 million inhabitants expected in the region by 2080 under this scenario. These results underscore the increasing territorial disparities in water availability and highlight the urgent need for differentiated and basin-specific management strategies to mitigate water stress in the face of growing climatic and demographic pressures.

Aggregate indicators based on renewable water resources only reflect long-term averages and do not capture the spatial heterogeneity of pressures or the effects of infrastructure or climate-induced variability on actual water availability. Moreover, conditions are expected to deteriorate over time in many subregions. For this reason, it is essential to examine potential water availability in conjunction with basic pressure indicators, namely, population density and irrigated area, to gain a better understanding of local vulnerabilities and the capacity to adapt to future hydrological constraints across the Mediterranean basin.

Fig. 11 presents the spatial distribution of average per capita water availability in the Mediterranean basins for two time periods and multiple scenarios. The top panel illustrates the current situation, based on the average values of potential water availability from the H08 and CWatM hydrological models under the *obsclim* scenario for the period 1980–2019. The three lower panels show projections for the period 2060–2099 under the SSP1–2.6, SSP3–7.0, and SSP5–8.5 scenarios, respectively, averaged across all available climate projections. In the reference period (*obsclim*), the average per capita water availability in the region is estimated at 430 m^3 / person/year. By the late 21st century, this value is projected to decrease across all scenarios, with estimated availabilities of 367 m^3 / person/year under SSP1–2.6, 223 m^3 /person/year under SSP3–7.0, and 227 m^3 /person/year under SSP5–8.5. These declines result from the combined effects of climate change and population growth.

Notably, the most critical decline in per capita availability does not occur under the most extreme climate scenario (SSP5–8.5, where water availability is expected to decrease by 41.05 %), but under SSP3–7.0, where the projected reduction in potential water availability is more moderate (34.04 %). This is explained by demographic factors: in SSP3–7.0, the population of the Mediterranean basin is projected to increase by 31 %, whereas in SSP5–8.5, the increase is only 15 %. This interplay between climate and demographic trends underscores the importance of integrated assessments that consider both hydrological impacts and socioeconomic dynamics when evaluating future water stress.

Figure S7 explores the relationship between potential water availability and the population of each basin included in the model. Structurally analogous to Fig. 10, this figure highlights three threshold values of potential water availability: 1000 m^3 , 500 m^3 , and 100 m^3 per person per year. These benchmarks help contextualize the implications of water scarcity under varying scenarios. Notably, if the total potential availability were dedicated exclusively to urban consumption, the lowest threshold, 100 m^3 per person per year, would correspond to approximately 274 liters per person per day, a value aligned with typical water use in Mediterranean urban areas. In the current situation (*obsclim*, 1980–2019), only 12 basins (3 %) fall below these critical thresholds, but they hold a substantial share of the population: about 22 % of the 199 million inhabitants lives in basins where potential water availability does not exceed 100 m^3 per person per year. This already points to acute limitations in terms of water security under existing climatic and demographic conditions. Under the most adverse climate and population scenario (SSP3–7.0, 2060–2099), the number of affected basins and population exposure intensifies markedly. The number of basins falling below the lowest threshold increases to 29 (8 %), and the population living under conditions of low potential water availability rises to 114 million people, representing 44 % of the 262 million projected inhabitants. This stark increase reflects the compound effect of declining hydrological inputs and demographic growth, underscoring the escalating challenge of ensuring sufficient water supply under future climate and socioeconomic trajectories.

These results illustrate how combining climate projections with indicators of potential availability provides a valuable lens for identifying areas of heightened vulnerability. They emphasize the necessity of adopting spatially differentiated adaptation strategies that account for both natural and anthropogenic pressures on water resources.

With regard to agricultural use, the average potential water availability across the Mediterranean basins is estimated in the *obsclim* scenario at 14,497 m^3 per hectare of irrigated land per year. This figure indicates, in general terms, sufficient water to support the intensive agricultural practices currently prevalent in the region. However, spatial disparities are evident and merit closer examination. Fig. 12 presents the spatial distribution of average water availability per hectare of irrigated land. The top panel corresponds to the reference period under the *obsclim* scenario (1980–2019), while the three lower panels display projected conditions for the period 2060–2099 under the SSP1–2.6, SSP3–7.0, and SSP5–8.5 scenarios. In the most adverse projection (SSP5–8.5), average availability

declines to 8820 m^3 per hectare per year, reflecting a substantial reduction in renewable resources available for irrigation. Importantly, even under current conditions, several basins exhibit relatively low water availability per hectare, suggesting that certain regions already operate under high pressure and may face critical constraints in the future. These localized deficits become more

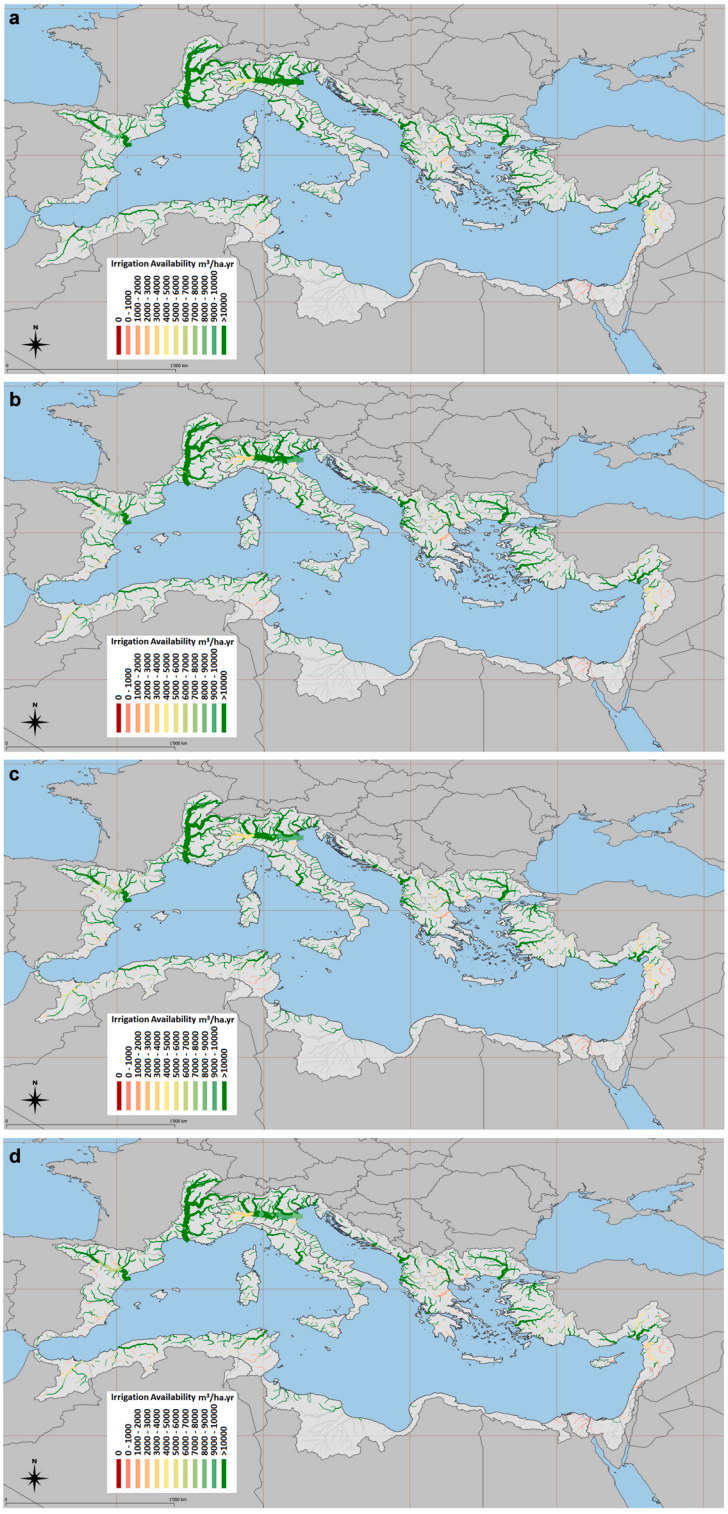

Fig. 12. Spatial distribution of the average water availability per hectare in the Mediterranean basin. a: *obsclim* scenario. b: SSP1–2.6 scenario in 2060–2099. c: SSP3–7.0 scenario in 2060–2099. d: SSP5–8.5 scenario in 2060–2099.

pronounced under climate change scenarios, highlighting the uneven distribution of vulnerability and the necessity of tailoring adaptation strategies to basin-specific hydrological and agricultural contexts.

Figure S8 illustrates the relationship between irrigated area and potential water availability across the Mediterranean basins, following the same structure as Figures 10 and S7. The reference lines represent threshold values of 10,000, 5000, and 2000 m^3 per hectare per year, offering a visual benchmark for assessing the adequacy of water availability for irrigation purposes. The results reveal a subset of agricultural areas where the average potential endowment per hectare is relatively low, even under current conditions. Out of the 363 modeled basins, 333 contain irrigated land. In the reference scenario (*obsclim*), 23 basins, equivalent to 7 % of the irrigated basins, show availability below 2000 m^3 /hectare/year, while another 30 basins (9 %) fall within the 2000–5000 m^3 /hectare/year range. In total, 16 % of the irrigated basins fall below the 5000 m^3 /hectare/year threshold. These areas collectively account for 2.02 million hectares, representing approximately 34 % of the total irrigated area in the region.

Under the most adverse future projection (SSP3–7.0, 2060–2099), the number of water-stressed basins increases notably. In this scenario, 40 basins (12 %) register availability below 2000 m^3 /hectare/year, and 47 basins (14 %) fall within the intermediate range of 2000–5000 m^3 /hectare/year. Altogether, 26 % of the irrigated basins would experience availability below 5000 m^3 /hectare/year, with a combined irrigated area of 2.46 million hectares, 42 % of the irrigated basins. These findings highlight specific basins where agricultural water use is already under strain or likely to become so under future conditions. Targeted interventions to improve water use efficiency, optimize cropping patterns, and enhance agronomic planning will be essential to bolster the resilience of irrigated agriculture in these vulnerable regions.

Fig. 13 provides a synthetic summary of the spatial disparities in water availability relative to population and irrigated area across the Mediterranean basins. It presents three cumulative distribution plots for the 363 modeled basins, each representing a different metric of water pressure under current and future climate conditions (2060–2099). The top-left panel illustrates per capita water availability based on total renewable water resources, while the top-right panel shows per capita availability derived from potential (regulated) water availability. The bottom panel displays the distribution of potential water availability per hectare of irrigated land. In each case, the basins are sorted by increasing availability, and the corresponding cumulative population or irrigated area is plotted, highlighting the share of people or agricultural land exposed to varying degrees of water scarcity. This format facilitates a comparative analysis of the three SSP scenarios (SSP1–2.6, SSP3–7.0, and SSP5–8.5), illustrating how changes in climate, combined with population growth and agricultural water demand, may shift a substantial portion of the Mediterranean territory into conditions of increasing water stress.

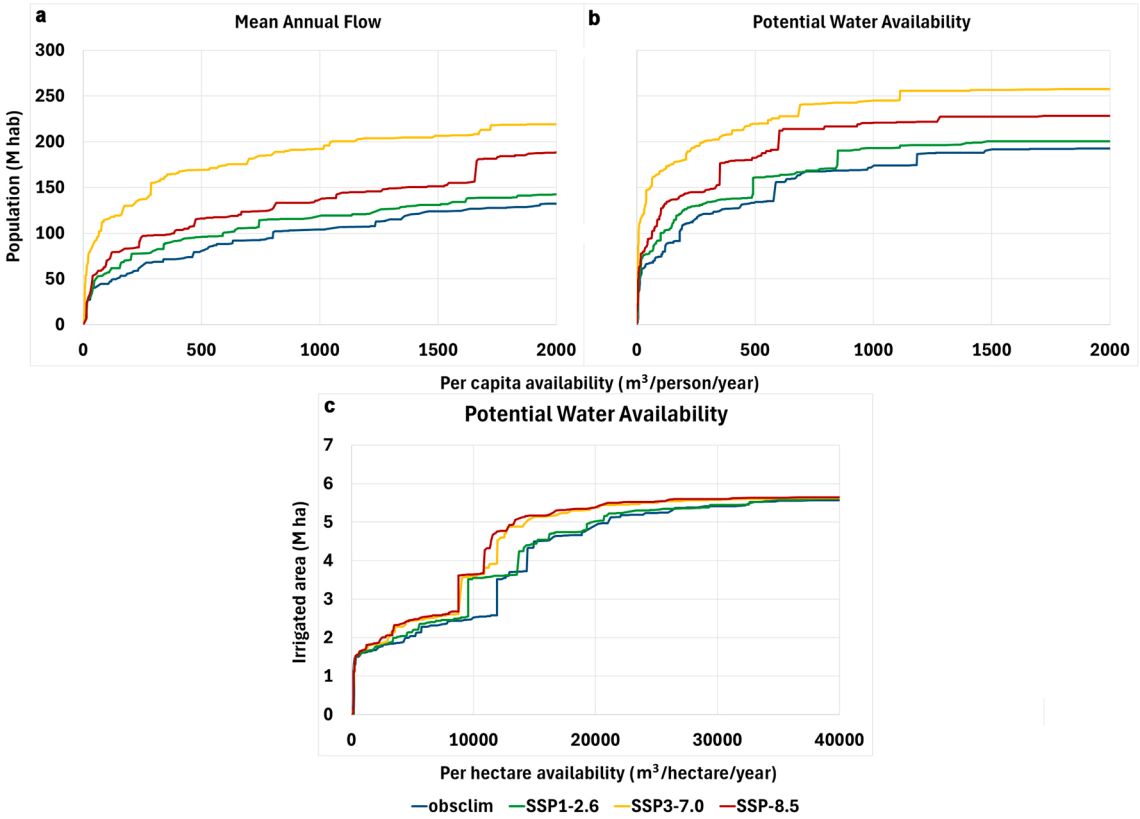

Fig. 13. Distribution of unit availability in the *obsclim* and future scenarios in 2060–2100. a: Per capita availability based on renewable water resources. b: Per capita availability based on potential water availability. c: Per hectare availability based on potential water availability.

The results presented in Fig. 13 clearly illustrate how the combined pressures of climate change and demographic growth exacerbate water scarcity across the Mediterranean region. When examining per capita availability based on total renewable water resources, the number of people with less than 500 m^3 /person/year increases from 81 million in the *obsclim* scenario to 169 million in the most unfavorable future scenario (SSP3–7.0), more than a twofold increase. For per capita availability based on potential (regulated) water availability, using a threshold of 100 m^3 /person/year, representing a reasonable volume required for basic urban supply, the population exposed to scarcity increases from 75 million in the *obsclim* scenario to 168 million in SSP3–7.0, a 125 % increase. This result highlights that the impact of climate change on effective water availability is even greater than that observed for mean annual flows. In the case of availability for irrigation, using 5000 m^3 /hectare/year as a threshold for scarcity, the irrigated area considered under-supplied increases from 2.04 million hectares in the *obsclim* scenario to 2.47 million hectares in SSP5–8.5, a 21 % increase. These are substantial increases, particularly for per capita indicators, and they emphasize the growing vulnerability of water-dependent systems. The clear separation between the curves corresponding to different scenarios underscores the significant impact that future developments may have on water availability and the need for proactive adaptation strategies.

These findings reinforce the need for territorially differentiated and forward-looking water management strategies. The sharp increases in the population and irrigated land exposed to water scarcity thresholds suggest that relying on current infrastructure and management practices will be insufficient to maintain supply reliability under future climate and demographic scenarios. Adaptation will require not only improving efficiency in water use, particularly in the agricultural sector, but also enhancing the flexibility of allocation systems, protecting environmental flows, and investing in alternative water sources, such as reuse and desalination. Moreover, the results underscore the importance of integrating climate projections, demographic trends, and infrastructure assessments into water planning frameworks. Policymakers must prioritize vulnerable basins and sectors, promote resilience through diversification, and ensure that future water strategies are informed by spatially explicit, scenario-based analyses such as the one presented in this study.

4.4. Limitations of the analysis

While the results presented in this study offer valuable insights into the future availability of water in Mediterranean basins under climate change, they are subject to several limitations that should be acknowledged to properly contextualize their scope and implications. These limitations can be grouped into four main categories: (i) those related to hydrological modeling and the representation of natural flows; (ii) those associated with the simulation of water management processes performed by the WAAPA model; (iii) those derived from the assumptions made in future projections of climate and socio-economic drivers; and (iv) those concerning the indicators used to synthesize the results and evaluate water scarcity.

The first group of limitations concerns the hydrological basis of the analysis. River flow series constitute the fundamental input data, but the absence of regionally calibrated hydrological models required the use of two global hydrological models (H08 and CWatM) which, despite their validated performance, inevitably simplify key hydrological processes. Regional calibration is limited, and model accuracy can vary considerably across basins due to differences in physiographic and climatic conditions.

The performance levels of H08 and CWatM are comparable to those of other state-of-the-art global hydrological models and confirm the suitability of the models for large-scale climate impact assessments. However, the transferability of parameter sets to smaller or more heterogeneous Mediterranean basins introduces additional uncertainty. For this reason, our analysis emphasizes relative changes and spatial patterns rather than absolute discharge values

Validation of the global hydrological models was constrained by the limited availability of direct observations of natural (unregulated) flows in the Mediterranean region. Most major rivers are heavily altered by human regulation, and observed discharge data reflect operational water management rather than natural hydrological conditions. For this reason, direct comparison with gauge records would not provide meaningful validation. Instead, the outputs of the global hydrological models (H08 and CWatM) were compared against national-scale naturalized flow models, SIMPA in Spain and BIGBANG in Italy, which are high-resolution, locally calibrated hydrological models used in official water planning processes. Although these models are themselves simplified representations of the hydrological cycle, they constitute the most detailed and credible regional references available. The consistency observed between global and regional models, particularly in large basins such as the Ebro and Po, supports the reliability of global models for reproducing long-term trends and spatial patterns of flow. Nonetheless, the study acknowledges that such model-based validation cannot eliminate all uncertainty, and therefore, the interpretation of results focuses primarily on relative variations and spatial contrasts rather than on absolute values of discharge or availability.

The analyses presented in this paper focus on representative basins larger than 14,000 km^2, where the scale compatibility between model resolution and basin extent is more adequate. In the validation exercise performed for six large basins located in Spain and Italy, where higher-resolution national models (SIMPA, 500 m; BIGBANG, 1 km) are available, the global model results showed acceptable agreement in terms of mean annual flow and interannual variability. Therefore, although we acknowledge the limitations inherent to the coarse resolution of global models, the consistency observed in the comparative analysis supports the validity of the results at the regional scale considered.

One limitation of this study lies in the differences between the runoff volumes simulated by the two global hydrological models used. Under the *obsclim* scenario, the total simulated runoff differs by nearly 20 % (288 vs. 346 km^3/year for H08 and CWatM, respectively). This discrepancy reflects uncertainties related to model calibration, parameterization, and representation of hydrological processes at global scale. In the absence of consistent regional observations of natural flow, it is not possible to determine which model provides a more accurate estimate. Nevertheless, both models yield comparable spatial distributions and temporal variability, which supports the robustness of the multi-model mean adopted in this analysis. The use of ensemble averages has been shown in

previous studies to mitigate model-specific biases and to provide more reliable large-scale assessments of climate change impacts on water resources.

The second group of limitations relates to the simplified representation of water management in the WAAPA model. This model relies on globally available data and simulates only surface water dynamics, without explicitly considering groundwater interactions, infrastructure performance, or country-specific management practices. While suitable for comparative assessments, this model does not fully capture the complexity of real-world institutional, operational, or legal frameworks governing water use at the basin level. As a result, the estimated potential water availability should be interpreted as an approximation based on standardized management assumptions rather than actual operational conditions.

The modeling framework of this study does not account explicitly for water conveyance networks or interbasin transfer infrastructure. The Mediterranean water system is characterized not only by extensive reservoir regulation but also by a network of canals, pipelines, and aqueducts that redistribute water over long distances to supply urban centers and irrigated areas. Due to the lack of harmonized and publicly available data on the location, capacity, and operational rules of these transfer systems, the model assumes that allocation occurs within each basin. This simplification may affect local accuracy, particularly in basins with significant transfers such as the Tagus-Segura system in Spain. Nevertheless, the impact of this limitation is reduced at regional and sub-basin scales, since the results presented for representative basins correspond to larger drainage units that integrate the main water flows. The basin-level balances can therefore be considered robust, even though the spatial distribution maps of water availability and pressure should be interpreted with caution in areas where interbasin conveyance plays an important role.

A key limitation is that the study focuses exclusively on surface water availability, while groundwater resources have not been explicitly assessed. Incorporating groundwater would require detailed information on aquifer boundaries, recharge rates, and sustainable extraction thresholds, which are not available at the resolution and spatial coverage used in this analysis. This simplification may affect the completeness of the water scarcity diagnosis in regions heavily reliant on aquifers for irrigation and urban supply.

Nevertheless, the results provide a consistent framework for comparing surface water availability across Mediterranean basins and highlight the importance of integrated water resources management. The joint consideration of surface, groundwater, and non-conventional resources, such as desalinated and reclaimed water, represents a key pathway to enhance water security and resilience in the region. Future research should therefore aim to couple the WAAPA model with groundwater balance assessments and incorporate non-conventional sources to provide a more comprehensive picture of water availability under changing climate and demand conditions.

Finally, a third group of limitations derives from the scope of the future scenarios used. The analysis incorporates projections of climate forcing and population growth but maintains other socio-economic drivers, such as agricultural evolution, technological improvements, and adaptive management strategies, as constant. This assumption reduces the realism of the future projections but allows isolating the direct effects of climate and demographic change on water availability.

The study is constrained by uncertainties inherent in the climate forcing data provided by the ISIMIP3b dataset. Although using an ensemble of climate projections helps reduce model-specific biases, outputs remain sensitive to the choice of climate model, downscaling method, and emissions pathway. Similarly, the socio-economic projections, particularly those concerning population growth, are based on scenario assumptions that may not reflect actual future trajectories. The analysis also does not incorporate potential changes in irrigated land extent, such as expansion or abandonment, which could play a decisive role in shaping future water demands in Mediterranean agriculture, especially under changing political, economic, or technological conditions.

Additionally, the analysis assumes static water management behaviors and infrastructure throughout the projection periods. It does not account for potential adaptive responses, including improvements in irrigation efficiency, changes in cropping patterns, expanded use of non-conventional water sources (e.g., desalination or wastewater reuse), or institutional reforms aimed at improving allocation efficiency. These factors could substantially alter the balance between availability and demand, particularly in regions with strong adaptive capacity. Therefore, further research is needed to explore the influence of other key determinants of water demand, such as changes in irrigated area, economic development, technological improvements, and water use efficiency. Ongoing work is addressing some of these aspects through the estimation of current and future irrigation water requirements across the Mediterranean, using crop distribution maps instead of irrigated area statistics. This approach will allow the assessment of alternative cropping patterns and management strategies aimed at reducing agricultural water demand. Although such analyses are beyond the scope of the present study, they represent a natural continuation of this work and will contribute to developing more effective policies for water management and scarcity mitigation in the region.

A final group of limitations concerns the indicators adopted to summarize and compare results across basins. The indicators of availability per capita and per hectare of irrigated land provide a useful first approximation of potential pressure on water resources. However, it is important to emphasize that these indicators were derived independently, based on total available water, without considering the competition among different water uses. In practice, water availability must be simultaneously allocated to domestic supply, irrigated agriculture, and environmental flow requirements, along with other consumptive and non-consumptive uses. Therefore, the values obtained should be interpreted as theoretical upper limits, and not summed or compared without considering such competition. Under conditions of increasing pressure, the simultaneous and often conflicting demands on limited water resources become a critical management challenge, especially in regions where demands are spatially or temporally concentrated.

The present analysis should not be interpreted as a comprehensive diagnosis of water scarcity in the region. Such a diagnosis would require more detailed modeling that accounts for storage and conveyance infrastructure, groundwater use, and the full set of operational rules governing basin management. These mechanisms play a crucial role in ensuring supply reliability, which in many Mediterranean regions remains adequate under current conditions despite physical scarcity. Our modeling framework offers a consistent and spatially explicit basis for regional comparison. However, its results cannot be directly applicable to local water

management without further refinement. Planning at regional or basin level would benefit from downscaling, stakeholder consultation, and integration of governance and institutional factors not addressed in this study.

Despite these limitations, incorporating projected changes in climate and population into the analysis reveals concerning trends. As shown in previous sections, in the most extreme scenario (SSP5–8.5, for the 2060–2099 period), potential water availability declines by up to 41 % compared to the baseline, with water pressure indicators worsening by up to 50 % when population growth is also considered. The findings suggest that current difficulties in balancing water uses locally may intensify significantly in the future, reinforcing the urgency of managing water with principles of efficiency, equity, and resilience. The results point to the need for integrated and adaptive water governance, emphasizing flexible allocation, protection of environmental flows, and improvements in water use efficiency.

Finally, the analysis underscores the importance of developing and using spatially explicit information systems, such as the one presented in this study, to support evidence-based decision-making and to anticipate areas of heightened vulnerability. Future research should build on this work by incorporating seasonal variability, detailed management practices, and explicit adaptation pathways to more effectively inform policy responses under conditions of uncertainty.

5. Conclusions

This study presents an integrated assessment of potential water availability in Mediterranean river basins under a range of future climate scenarios. By combining simulations from two global hydrological models (H08 and CWatM) with the WAAPA water allocation model, the analysis captures both climate-driven hydrological changes and the moderating effects of reservoir infrastructure and management practices. The results offer a detailed and spatially explicit picture of how water availability in the region may evolve over the twenty-first century, with important implications for adaptation planning and resource governance.

The simulations reveal a consistent and robust decline in average annual streamflow across Mediterranean basins, with reductions of up to 26 % projected under the SSP5–8.5 scenario for the 2060–2099 period. This hydrological decline is further amplified when translated into potential water availability, which could decrease by as much as 41 % under the same scenario. The results also underscore the essential role of reservoirs in buffering interannual variability and sustaining supply. Under current conditions, more than half (53 %) of potential water availability is attributable to existing storage infrastructure. In its absence, the ability to meet present demands would be severely compromised, particularly during dry years or periods of peak consumption.

Beyond mean flow reductions, the study highlights an increase in interannual hydrological variability, by up to 31 % in the most adverse scenarios, which further undermines the reliability of water supply. This added instability increases vulnerability to extreme events such as prolonged droughts, especially in regions with limited regulation capacity. Spatial disparities are also significant: basins with low storage, greater seasonality, or high demand intensity face disproportionately greater reductions in availability, suggesting the need for territorially differentiated adaptation responses.

The methodological framework used in this study demonstrates the value of integrating global hydrological projections with reservoir simulation tools. WAAPA enables the estimation of operationally defined water availability by accounting for storage dynamics, evaporation, ecological flow requirements, and demand prioritization. This approach provides a more realistic and actionable basis for planning than indicators based solely on natural runoff or climatic variables.

The findings underscore the urgency of incorporating climate change explicitly into hydrological planning and investment strategies across the Mediterranean. Key priorities include protecting and optimizing existing infrastructure, improving efficiency in both urban and agricultural water use, and designing adaptive measures that enhance resilience to both long-term trends and short-term extremes. Moreover, the development of spatially explicit decision-support tools, as demonstrated in this study, is essential for identifying critical hotspots and supporting evidence-based policymaking under uncertainty.

Future research should aim to incorporate groundwater and alternative water sources (e.g., desalination, wastewater reuse), provide a more detailed representation of water allocation requirements (including environmental flows, urban supply, irrigation, tourism and other uses), and account for adaptive capacity, such as demand-side adjustments and evolving institutional frameworks. Nonetheless, the current analysis offers a robust foundation for understanding the magnitude and spatial distribution of climate-related risks to water availability in one of the world's most vulnerable regions.

CRediT authorship contribution statement

Ana Iglesias: Writing – review & editing, Validation, Supervision, Funding acquisition, Conceptualization. **Alvaro Sordo-Ward:** Writing – review & editing, Validation, Software, Methodology. **Luis Garrote:** Writing – original draft, Visualization, Software, Methodology, Conceptualization. **Francisco Martin-Carrasco:** Writing – review & editing, Validation, Supervision, Conceptualization. **Paola Bianucci:** Writing – review & editing, Validation, Methodology, Data curation.

Declaration of Competing Interest

The authors declare that they have no known competing financial interests or personal relationships that could have appeared to influence the work reported in this paper.

Acknowledgements

This research was carried out within the AG-WaMED project, funded by the Partnership for Research and Innovation in the Mediterranean Area Programme (PRIMA), an Art 185 initiative supported and funded under Horizon 2020, the European Union's Framework Programme for Research and Innovation, Grant Agreements: Italy: 391 of 20/10/2022, Egypt: 45878, Tunisia: 0005874–004–18–2022–3, Greece: ΓΓΡ21–0474657, Spain: PCI2022–132929. We would like to thank the rest of the AG-WaMED team for their fruitful discussions, which played a significant role in refining our ideas and shaping the final work. This study utilized input data from HydroSheds, GRUMP, GMIA and ISIMIP3b (impact models H08 and CWatM). We acknowledge the data providers for their contributions.

During the preparation of this manuscript/study, the authors used Writefull for Word and ChatGPT, version 4 for the purposes of proofreading, grammar and style correction. The authors have reviewed and edited the output and take full responsibility for the content of this publication.

Appendix A. Supporting information

Supplementary data associated with this article can be found in the online version at doi:10.1016/j.ejrh.2025.102960.

Data availability

Data used for the research were downloaded from publicly available sources that have been properly identified

References

Andreu, J., Capilla, J., Sanchís, E., 1996. AQUATOOL, a generalized decision-support system for water-resources planning and operational management. J. Hydrol. 177 (3-4), 269–291. https://doi.org/10.1016/0022-1694(95)02963-X.

Arjdal, K., Driouech, F., Vignon, É., Chéruy, F., Manzanas, R., Drobinski, P., Chehbouni, A., Idelkadi, A., 2023. Future of land surface water availability over the Mediterranean basin and North Africa: analysis and synthesis from the CMIP6 exercise. Atmos. Sci. Lett. 24 (11), e1180. https://doi.org/10.1002/asl.1180.

Ben-Salem, N., Reinecke, R., Copty, N.K., Gómez-Hernández, J., Varouchakis, E.A., Karatzas, G.P., Rode, M., Jomaa, S., 2023. Mapping steady-state groundwater levels in the Mediterranean region: the Iberian Peninsula as a benchmark. J. Hydrol. 626, 130207. https://doi.org/10.1016/j.jhydrol.2023.130207.

Bianucci, P., Sordo-Ward, A., Lama-Pedrosa, B., Garrote, L., 2024. How do environmental flows impact on water availability under climate change scenarios in European basins? Sci. Total Environ. 911 (2024), 168566. https://doi.org/10.1016/j.scitotenv.2023.168566.

Braca, G., Bussettini, M., Gafà, R.M., Monti, G.M., Martarelli, L., Silvi, A., La Vigna, F., 2022. The nationwide water budget estimation in the light of the new Permeability map of Italy. Acque Sotter. Ital. J. Groundw. 11 (3), 31–39. https://doi.org/10.7343/as-2022-575.

Braca G., Bussettini M., Lastoria B., Mariani S., Piva F. (2021) Il Bilancio Idrologico Gis BAsed a scala Nazionale su Griglia regolare - BIGBANG: metodologia e stime. Rapporto sulla disponibilità naturale della risorsa idrica. Istituto Superiore per la Protezione e la Ricerca Ambientale, Rapporti 339/21, Roma. Retrieved from: ⟨https://www.isprambiente.gov.it/files2021/pubblicazioni/rapporti/rapporto_ispra_339-21_bigbang_ld.pdf⟩. Accessed on 01/30/2025.

Burek, P., Satoh, Y., Kahil, T., Tang, T., Greve, P., Smilovic, M., Guillaumot, L., Zhao, F., Wada, Y., 2020. Development of the Community Water Model (CWatM v1.04) - a high-resolution hydrological model for global and regional assessment of integrated water resources management. Geosci. Model Dev. 13 (7), 3267–3298. https://doi.org/10.5194/gmd-13-3267-2020.

Burek, P., Smilovic, M., 2023. The use of GRDC gauging stations for calibrating large-scale hydrological models. Earth Syst. Sci. Data 15 (12), 5617–5629. https://doi.org/10.5194/essd-15-5617-2023.

Casadei, S., Peppoloni, F., Pierleoni, A., 2020. A New Approach to Calculate the Water Exploitation Index (WEI+). Water 12 (11), 3227. https://doi.org/10.3390/w12113227.

CEDEX. (2020). Evaluación de recursos hídricos en régimen natural en España (1940/41 - 2017/18). Ministerio de Fomento y Ministerio para la Transición Ecológica. Retrieved from: ⟨https://www.miteco.gob.es/content/dam/miteco/es/agua/temas/evaluacion-de-los-recursos-hidricos/cedex-informeerh2019_tcm30-518171.pdf⟩. Acecessed on 05/19/2021.

Cramer, W., Guiot, J., Fader, M., Garrabou, J., Gattuso, J.-P., Iglesias, A., Lange, M.A., Lionello, P., Llasat, M.C., Paz, S., Peñuelas, J., Snoussi, M., Toreti, A., Tsimplis, M.N., Xoplaki, E., 2018. Climate change and interconnected risks to sustainable development in the Mediterranean. Nat. Clim. Change. https://doi.org/10.1038/s41558-018-0299-2.

Dorado-Guerra, D.Y., Paredes-Arquiola, J., Pérez-Martín, M.Á., Corzo-Pérez, G., Ríos-Rojas, L., 2023. Effect of climate change on the water quality of Mediterranean rivers and alternatives to improve its status. J. Environ. Manag. 348, 119069. https://doi.org/10.1016/j.jenvman.2023.119069.

Dunne, J.P., Horowitz, L.W., Adcroft, A.J., Ginoux, P., Held, I.M., John, J.G., Krasting, J.P., Malyshev, S., Naik, V., Paulot, F., et al., 2020. The GFDL earth system model version 4.1 (GFDL-ESM 4.1): overall coupled model description and simulation characteristics. J. Adv. Model. Earth Syst. 12 (11), e2019MS002015. https://doi.org/10.1029/2019MS002015.

Eekhout, J.P.C., Nunes, J.P., Tramblay, Y., de Vente, J., 2025. Severe impacts on water resources projected for the Mediterranean Basin. Wiley Interdiscip. Rev. Water 12 (2), e70012. https://doi.org/10.1002/wat2.70012.

Eng, K., Medalie, L., Skinner, K.D., Ivahnenko, T.I., Heilman, J.A., Smith, J.D., 2025. Predictability and behavior of water transfers across basin boundaries. JAWRA J. Am. Water Resour. Assoc. 61 (1), e13250. https://doi.org/10.1111/1752-1688.13250.

Estrela, T., Quintas, L., 1996. El sistema integrado de modelización precipitación-aportación SIMPA. Ing. ía Civ. 104, 43–52.

Fader, M., Shi, S., von Bloh, W., Bondeau, A., Cramer, W., 2016. Mediterranean irrigation under climate change: More efficient irrigation needed to compensate for increases in irrigation water requirements. Hydrol. Earth Syst. Sci. 20 (2), 953–973. https://doi.org/10.5194/hess-20-953-2016.

Falkenmark, M., Lundqvist, J., Widstrand, C., 1989. Macro-scale water scarcity requires micro-scale approaches. Nat. Resour. Forum 13 (4), 258–267. https://doi.org/10.1111/j.1477-8947.1989.tb00348.x.

Gain, A.K., Giupponi, C., Wada, Y., 2016. Measuring global water security towards sustainable development goals. Environ. Res. Lett. 11, 124015. https://doi.org/10.1088/1748-9326/11/12/124015.

González-Zeas, D., Garrote, L., Iglesias, A., Sordo-Ward, A., 2012. Improving runoff estimates from regional climate models: a performance analysis in Spain. Hydrol. Earth Syst. Sci. 16, 1709–1723. ⟨https://doir.org/10.5194/hess-16-1709-2012⟩.

Granados, A., Sordo-Ward, A., Paredes-Beltrán, B., Garrote, L., 2021. Exploring the Role of Reservoir Storage in Enhancing Resilience to Climate Change in Southern Europe. Water 13 (85), 1–22. https://doi.org/10.3390/w13010085.

Gupta, H.V., Kling, H., Yilmaz, K.K., Martinez, G.F., 2009. Decomposition of the mean squared error and NSE performance criteria: implications for improving hydrological modelling. J. Hydrol. 377 (1-2), 80–91. https://doi.org/10.1016/j.jhydrol.2009.08.003.

Gutjahr, O., Putrasahan, D., Lohmann, K., Jungclaus, J.H., von Storch, J.-S., Brüggemann, N., Haak, H., Stössel, A., 2019. Max planck institute earth system model (MPI-ESM1.2) for the high-resolution model intercomparison project (HighResMIP). Geosci. Model Dev. 12, 3241–3281. https://doi.org/10.5194/gmd-12-3241-2019.

Hanasaki, N., Kanae, S., Oki, T., Masuda, K., Motoya, K., Shirakawa, N., Shen, Y., Tanaka, K., 2008. An integrated model for the assessment of global water resources - Part 1: model description and input meteorological forcing. Hydrol. Earth Syst. Sci. 12 (4), 1007–1025. https://doi.org/10.5194/hess-12-1007-2008.

Hanasaki, N., Kanae, S., Oki, T., Masuda, K., Motoya, K., Shirakawa, N., Shen, Y., Tanaka, K., 2010. An estimation of global virtual water flow and sources of water for major crops and livestock products using a global hydrological model. J. Hydrol. 384 (3-4), 232–244. https://doi.org/10.1016/j.jhydrol.2009.09.028.

Harmanny, K.S., Malek, Ž., 2019. Adaptations in irrigated agriculture in the Mediterranean region: an overview and spatial analysis of implemented strategies. Reg. Environ. Change 19, 1401–1416. https://doi.org/10.1007/s10113-019-01494-8.

CIESIN (2017) Gridded Population of the World Version 4 (GPWv4): Population Density, revision 11 (Version 4.11)[Data set]. NASA Socioeconomic Data and Applications Center (SEDAC), Columbia University, Palisades, NY. https://doi.org/10.7927/H49C6VHW. Accessed on 04/06/2023.

ICOLD (2023) World Register of Dams. Retrieved from: ⟨http://www.icold-cigb.net/⟩. Accessed on: 07/09/2020.

Iglesias, A., Garrote, L., Flores, F., Moneo, M., 2007. Challenges to manage the risk of water scarcity and climate change in the Mediterranean. Water Resour. Manag. 21 (5), 775–788. https://doi.org/10.1007/s11269-006-9111-6.

Iglesias, A., Garrote, L., 2015. Adaptation strategies for agricultural water management under climate change in Europe. In: In Agricultural Water Management, 155. Elsevier, pp. 113–124. https://doi.org/10.1016/j.agwat.2015.03.014.

IPCC, 2022: Climate Change 2022: Impacts, Adaptation, and Vulnerability. Contribution of Working Group II to the Sixth Assessment Report of the Intergovernmental Panel on Climate Change (H.-O. Pörtner, D.C. Roberts, M. Tignor, E.S. Poloczanska, K. Mintenbeck, A. Alegría, M. Craig, S. Langsdorf, S. Löschke, V. Möller, A. Okem, B. Rama (eds.)). Cambridge University Press. Cambridge University Press, Cambridge, UK and New York, NY, USA, 3056 pp. https://doi.org/10.1017/9781009325844.

Jones, B., O'Neill, B.C., 2016. Spatially explicit global population scenarios consistent with the shared socioeconomic pathways. Environ. Res. Lett. 11 (2016), 084003. https://doi.org/10.1088/1748-9326/11/8/084003.

Kummu, M., Ward, P.J., de Moel, H., Varis, O., 2016. Is physical water scarcity a new phenomenon? Global assessment of water shortage over the last two millennia. Environ. Res. Lett. 5 (3), 034006. https://doi.org/10.1088/1748-9326/5/3/034006.

Labadie, J.W., (2006) MODSIM: Decision Support System for Integrated River Basin Management. International Congress on Environmental Modelling and Software. 242. Burlington, Vermont, USA - July 2006.

Lehner, B., Liermann, C.Reidy, Revenga, C., Vörösmarty, C., Fekete, B., Crouzet, P., Döll, P., Endejan, M., Frenken, K., Magome, J., Nilsson, C., Robertson, J.C., Rodel, R., Sindorf, N., Wisser, D., 2011. High-resolution mapping of the world's reservoirs and dams for sustainable river-flow management. Front. Ecol. Environ. 9 (9), 494–502. https://doi.org/10.1890/100125.

Lehner, B., Verdin, K., Jarvis, A., 2008. New global hydrography derived from spaceborne elevation data. Eos Trans. Am. Geophys. Union 89 (10), 93–94. https://doi.org/10.1029/2008eo100001.

Lionello, P., Scarascia, L., 2018. The relation between climate change in the Mediterranean region and global warming. Reg. Environ. Change 18 (5), 1481–1493. https://doi.org/10.1007/s10113-018-1290-1.

Liu, J., Yang, H., Gosling, S.N., Kummu, M., Flörke, M., Pfister, S., Hanasaki, N., Wada, Y., Zhang, X., Zheng, C., Alcamo, J., Oki, T., 2017. Water scarcity assessments in the past, present, and future. Earth'S. Future 5 (6), 545–559. https://doi.org/10.1002/2016EF000518.

Mariotti, A., Pan, Y., Zeng, N., Alessandri, A., 2015. Long-term climate change in the Mediterranean region in the midst of decadal variability. Clim. Dyn. 44 (5-6), 1437–1456. https://doi.org/10.1007/s00382-015-2487-3.

Milano, M., Ruelland, D., Fernandez, S., Dezetter, A., Fabre, J., Servat, E., Fritsch, J.M., Ardoin-Bardin, S., Thivet, G., 2013. Current state of Mediterranean water resources and future trends under climatic and anthropogenic changes. Hydrol. Sci. J. 58 (3), 498–518. https://doi.org/10.1080/02626667.2013.774458.

Mulligan, M., van Soesbergen, A., Sáenz, L., 2020. GOODD, a global dataset of more than 38,000 georeferenced dams. Sci. Data 7, 31. https://doi.org/10.1038/s41597-020-0362-5.

Nash, J.E., Sutcliffe, J.V., 1970. River flow forecasting through conceptual models part I:a discussion of principles. J. Hydrol. 10 (3), 282–290. https://doi.org/10.1016/0022-1694(70)90255-6.

Noto, L.V., Cipolla, G., Pumo, D., Francipane, A., 2023. Climate change in the mediterranean basin (Part II): a review of challenges and uncertainties in climate change modeling and impact analyses. Water Resour. Manag. 37 (6-7), 2307–2323. https://doi.org/10.1007/s11269-023-03444-w.

O'Neill, B.C., Kriegler, E., Ebi, K.L., Kemp-Benedict, E., Riahi, K., Rothman, D.S., van Ruijven, B.J., van Vuuren, D.P., Birkmann, J., Kok, K., Levy, M., Solecki, W., 2017. The roads ahead: narratives for shared socioeconomic pathways describing world futures in the 21st century. Glob. Environ. Change 42, 169–180. https://doi.org/10.1016/j.gloenvcha.2015.01.004.

Paredes-Beltran, B.E., Sordo-Ward, Á., Martín-Carrasco, F., Garrote, L., 2024. High-resolution estimates of water availability for the Iberian Peninsula under climate scenarios. Appl. Water Sci. 14 (8). https://doi.org/10.1007/s13201-024-02165-8.

Pfister, S., Koehler, A., Hellweg, S., 2009. Assessing the environmental impacts of freshwater consumption in LCA. Environ. Sci. Technol. 43, 4098–4104 https://doi/10.1021/es802423e.

Plan Bleu (2008) The Blue Plan's sustainable development outlook for the Mediterranean. Retrieved from ⟨http://planbleu.org/sites/default/files/publications/upm_en_0.pdf⟩. Accessed 31 May 2025.

Raskin, P., Gleick, P., Kirshen, P., Pontius, G., & Strzepek, K. (1997). Comprehensive assessment of the freshwater resources of the world: State of the world report. Stockholm Environment Institute. Retrieved from: ⟨https://www.ircwash.org/sites/default/files/210-97CO-14039.pdf⟩. Accessed on 06/01/2025.

Seker, M., Gumus, V., 2022. Projection of temperature and precipitation in the Mediterranean region through multi-model ensemble from CMIP6. Atmos. Res. 280, 106440. https://doi.org/10.1016/J.ATMOSRES.2022.106440.

Sellar, A.A., Jones, C.G., Mulcahy, J.P., Tang, Y., Yool, A., Wiltshire, A., O'Connor, F.M., Stringer, M., Hill, R., Palmieri, J., Woodward, S., de Mora, L., Kuhlbrodt, T., Rumbold, S.T., Kelley, D.I., Ellis, R., Johnson, C.E., Walton, J., Abraham, N.L., Zerroukat, M., 2019. UKESM1: description and evaluation of the U.K. earth system model. J. Adv. Model. Earth Syst. 11 (12), 4513–4558. https://doi.org/10.1029/2019MS001739.

Sepulchre, P., Caubel, A., Ladant, J.-B., Bopp, L., Boucher, O., Braconnot, P., Brockmann, P., Cozic, A., Donnadieu, Y., Dufresne, J.L., et al., 2020. IPSL-CM5A2 - an Earth system model designed for multi-millennial climate simulations. Geosci. Model Dev. 13, 3011–3053. https://doi.org/10.5194/gmd-13-3011-2020, 2020.

Sieber, J. & Purkey, D. (2015) WEAP-Water Evaluation and Planning System: User Guide for WEAP, 2015. Stockholm Environment Institute-US Center, Somerville.

Siebert, S., Henrich, V., Frenken, K., & Burke, J. (2013). Update of the digital global map of irrigation areas to version 5. Rheinische Friedrich-Wilhelms-Universität Bonn, Alemania / Organización de las Naciones Unidas para la Agricultura y la Alimentación (FAO), Roma, Italia. Retrieved from: ⟨https://www.fao.org/aquastat/en/geospatial-information/global-maps-irrigated-areas/latest-version/⟩. Accessed on: 04/08/2023.

Sordo-Ward, A., Granados, I., Iglesias, A., Garrote, L., 2019. Blue water in Europe: estimates of current and future availability and analysis of uncertainty. Water 2019 11 (420), 1–18. https://doi.org/10.3390/w11030420.

Su, Q., Kambale, R.D., Tzeng, J.H., Amy, G.L., Ladner, D.A., Karthikeyan, R., 2025. The growing trend of saltwater intrusion and its impact on coastal agriculture: challenges and opportunities. Sci. Total Environ. 966, 178701. https://doi.org/10.1016/j.scitotenv.2025.178701.

Suárez-Almiñana, S., Solera, A., Madrigal, J., Andreu, J., Paredes-Arquiola, J., 2020. Risk assessment in water resources planning under climate change at the Júcar River basin, 2020 Hydrol. Earth Syst. Sci. 24, 5297–5315. https://doi.org/10.5194/hess-24-5297-2020.

Tramblay, Y., Llasat, M.C., Randin, C., Coppola, E., 2020. Climate change impacts on water resources in the Mediterranean. In: In Regional Environmental Change, 20. Springer, p. 83. https://doi.org/10.1007/s10113-020-01665-y.

Veldkamp, T.I.E., Wada, Y., Aerts, J.C.J.H., Döll, P., Gosling, S.N., Liu, J., Masaki, Y., Ostberg, S., Pokhrel, Y., Satoh, Y., Kim, H., Ward, P.J., 2017. Water scarcity hotspots travel downstream due to human interventions in the 20th and 21st century. Nat. Commun. 8 (1), 15697. https://doi.org/10.1038/ncomms15697.

Vicente-Serrano, S.M., Lopez-Moreno, J.I., Beguería, S., Lorenzo-Lacruz, J., Sanchez-Lorenzo, A., García-Ruiz, J.M., Azorin-Molina, C., Morán-Tejeda, E., Revuelto, J., Trigo, R., Coelho, F., Espejo, F., 2014. Evidence of increasing drought severity caused by temperature rise in southern Europe. Environ. Res. Lett. 9, 044001. https://doi.org/10.1088/1748-9326/9/4/044001.

Vörösmarty, C.J., Green, P., Salisbury, J., Lammers, R.B., 2010. Global water resources: vulnerability from climate change and population growth. Science 289 (5477), 284–288. https://doi.org/10.1126/science.289.5477.284.

Wada, Y., Wisser, D., Bierkens, M.F.P., 2014. Global modeling of withdrawal, allocation and consumptive use of surface water and groundwater resources. Earth Syst. Dyn. 5, 15–40. https://doi.org/10.5194/esd-5-15-2014.

Warszawski, L., Frieler, K., Huber, V., Piontek, F., Serdeczny, O., Schewe, J., 2014. The inter-sectoral impact model intercomparison project (ISI-MIP). Project framework. PNAS 111 (9), 3228–3232. ⟨https://www.pnas.org/doi/epdf/10.1073/pnas.1312330110⟩.

Weedon, G.P., Balsamo, G., Bellouin, N., Gomes, S., Best, M.J., Viterbo, P., 2014. The WFDEI meteorological forcing data set: WATCH forcing data methodology applied to ERA-interim reanalysis data. Water Resour. Res. 50 (9), 7505–7514. https://doi.org/10.1002/2014WR015638.

Yoshida, T., Hanasaki, N., Nishina, K., Boulange, J., Okada, M., Troch, P.A., 2022. Inference of parameters for a global hydrological model: identifiability and predictive uncertainties of climate-based parameters. Water Resour. Res. 58 (2), e2021WR030660. https://doi.org/10.1029/2021WR030660.

Smakhtin, V.U.; Revenga, C.; Doll, P. 2004. Taking into account environmental water requirements in global-scale water resources assessments. Colombo, Sri Lanka: International Water Management Institute (IWMI), Comprehensive Assessment Secretariat. v, 24p. Retrieved from: ⟨https://hdl.handle.net/10568/39741⟩. Accessed on 06/01/2025.

Yukimoto, S., Yoshimura, H., Hosaka, M., Sakami, T., Tanaka, T.Y., Shindo, E., Tsujino, H., Deushi, M., Mizuta, R., Yabu, S., Obata, A., Ose, T., & Kitoh, A. (2011) Meteorological Research Institute-Earth System Model Version 1 (MRI-ESM1) - Model Description. Technical Reports of the Meteorological Research Institute, No. 64. Tsukuba, Japan: Meteorological Research Institute, Japan Meteorological Agency. Retrieved from: ⟨https://www.mri-jma.go.jp/Publish/Technical/DATA/VOL_64/index_en.html⟩. Accessed 05/04/2023.

Zaherpour, J., Gosling, S.N., Mount, N., Schmied, H.M., Veldkamp, T.I.E., Dankers, R., Eisner, S., Gerten, D., Gudmundsson, L., Haddeland, I., Hanasaki, N., Kim, H., Leng, G., Liu, J., Masaki, Y., Oki, T., Pokhrel, Y., Satoh, Y., Schewe, J., Wada, Y., 2018. Worldwide evaluation of mean and extreme runoff from six global-scale hydrological models that account for human impacts. Environ. Res. Lett. 13 (6), 065015. https://doi.org/10.1088/1748-9326/aac547.